J. Fluid Mech. (1986), *vol.* 172, *pp.* 277–306
Printed in Great Britain

Stability of finite-amplitude interfacial waves. Part 3. The effect of basic current shear for one-dimensional instabilities

By D. I. PULLIN

Department of Mechanical Engineering, University of Queensland, St Lucia, Queensland, 4067 Australia

AND R. H. J. GRIMSHAW†

Department of Mathematics, University of Melbourne, Parkville, Victoria, 3052 Australia.

(Received 4 June 1985 and in revised form 13 February 1986)

We consider the linearized stability of interfacial progressive waves in a two-layer inviscid fluid, for the case when there is a basic current shear in either, or both, of the fluids. For this configuration the basic wave has been calculated by Pullin & Grimshaw (1983*b*). Our results here are mainly restricted to two-space-dimensional instabilities (i.e. one-dimensional in the propagation space), and are obtained both analytically and numerically. The analytical results are for the long-wavelength modulational instability of small-amplitude waves. The numerical results are restricted to the case when the lower fluid is infinitely deep, and for the Boussinesq approximation. They are obtained by solving the linearized stability problem with truncated Fourier series, and solving the resulting eigenvalue problem for the growth rate. For small values of the basic current shear, and for small or moderate basic wave amplitude, the instabilities are determined by a set of low-order resonances; for larger basic wave amplitude, these are dominated by the onset of a local wave-induced Kelvin–Helmholtz instability. For larger values of the basic current shear, this interpretation is modified owing to the appearance of a number of new effects.

1. Introduction

In two previous papers (Grimshaw & Pullin, 1985; Pullin & Grimshaw 1985, henceforth denoted I and II respectively) we studied the linearized stability of steady, progressive, periodic, finite-amplitude interfacial waves propagating on the interface between two fluids of densities ρ_1 and ρ_2, and undisturbed depths d_1 and d_2 respectively. The basic wave for these stability calculations was provided by the analytical and numerical solutions of Pullin & Grimshaw (1983*a*). In I and II we considered three space-dimensional perturbations to the basic wave describing a modulation with wavenumber (p, q). Here p is the wavenumber component in the direction of propagation of the basic wave, q is the transverse wavenumber component, and the modulation is two-dimensional in the propagation space. In I we used an analytical approximation for long-wave modulations (i.e. $|p|, |q| \ll |k_0|$ where k_0 is the wavenumber of the basic wave) when the basic wave amplitude δ is also small. The result was a nonlinear Schrödinger equation coupled to an equation for the

† Present address: School of Mathematics, University of N.S.W., P.O. Box 1, Kensington, N.S.W. 2033, Australia.

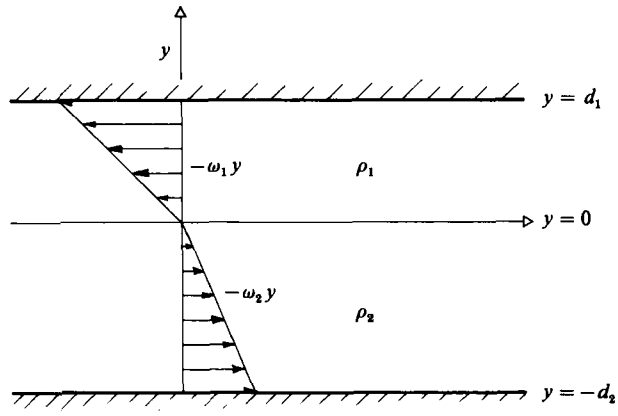

FIGURE 1. Basic current shear. Each layer contains fluid of constant density and uniform vorticity. The flow is bounded by rigid planes at $y = -d_2$, $y = d_1$.

wave-induced mean flow, from which the stability properties of the basic wave could be determined for the whole of the parameter space defined by the density ratio ρ_1/ρ_2 and $k_0 d_1$, $k_0 d_2$. In II we used numerical calculations to continue the results of I to finite values of the modulation wavenumber (p, q) and the basic wave amplitude δ for a restricted part of the parameter space ($k_0 d_2 \to \infty$, in the Boussinesq limit $\rho_1/\rho_2 \to 1$). I and II together showed that instability occurred in bands in the (p, q)-plane associated with a sequence of low-order resonances. Here the order of the resonance is N, where N components of the basic wave interact with two infinitesimal waves. No $N = 1$ resonances were found, but all the higher-order resonances ($N = 2$, 3, ...) occurred.

In this paper we consider the linearized stability of the non-uniform steady flow consisting of finite-amplitude interfacial waves on the basic current shown in figure 1. In each inviscid fluid the basic current has uniform vorticity ω_1 and ω_2 respectively corresponding to a basic horizontal current in the x-direction, $-\omega_1 y$ and $-\omega_2 y$ respectively. We note that if each of the fluid layers has a small but finite viscosity μ_j, in inverse proportion to their vorticities (i.e. $\mu_1 \omega_1 = \mu_2 \omega_2$), then the basic flow can be unstable to a viscous instability (e.g. Hooper & Boyd 1983). However, for very large Reynolds numbers this instability is confined to very short wavelengths which scale with the viscous diffusive length of one of the fluids, and are very much shorter than the typical wavelengths of atmospheric or oceanic internal waves. Moreover, this viscous instability has been established only for the unperturbed basic current shown in figure 1, and only when $\mu_1 \omega_1 = \mu_1 \omega_2$, and may not be applicable to the non-uniform steady flow due to the presence of finite-amplitude waves. Large-amplitude internal waves are commonly observed on the oceanic pycnocline, or on atmospheric inversion layers, often in the presence of an underlying shear flow, and these phenomena proved the major motivation and potential application for the present study. Interfacial waves for the configuration shown in figure 1 provide a relatively simple model to study the effect of basic current shear on wave stability. Yuen (1983) has studied the stability of interfacial waves for the case when there is a basic constant current $\bar{u}_j$, $j = 1, 2$, in each fluid, with a basic current jump $(\bar{u}_1 - \bar{u}_2)$ across the interface. However, unlike the present case, this basic current is subject to a short-wavelength Kelvin–Helmholtz (K–H) instability, which persists for waves of small amplitude. Here the steady, progressive, periodic, finite-amplitude wave

solutions were obtained both analytically and numerically by Pullin & Grimshaw (1983*b*). In the main we employ the same approach to wave stability used in I and II. However, because three space-dimensional perturbations to the basic wave are not vorticity-preserving, the stability calculations reported here are restricted to two-space-dimensional perturbations, which can be taken as irrotational. The modulations to the basic wave are thus one-dimensional in the propagation space and, in the terminology introduced above, the modulation wavenumber is $(p, 0)$ (i.e. $q = 0$). The one exception to this restriction occurs in §2, where we calculate the resonance curves for the full two-dimensional propagation space.

Relative to the basic current shear shown in figure 1, we let the perturbed flow have a velocity field $\boldsymbol{u}_j = (u_j, v_j, w_j)$ and a modified pressure $q_j = p_j + \rho_j g y$, $j = 1, 2$ in each fluid; p_j is the pressure. The inviscid equations of motion in each fluid are then

$$\frac{\partial \boldsymbol{u}_j}{\partial t} + (\boldsymbol{u}_j \cdot \nabla)\,\boldsymbol{u}_j - \omega_j y \frac{\partial \boldsymbol{u}_j}{\partial x} - \omega_j v_j \hat{\boldsymbol{x}} + \frac{1}{\rho_j}\nabla q_j = 0, \quad j = 1, 2. \tag{1.1}$$

We also assume that the flow is incompressible so that $\nabla \cdot \boldsymbol{u}_j = 0$, $j = 1, 2$. The boundary conditions at the disturbed interface, $y = \eta(x, z, t)$, are

$$\frac{\partial \eta}{\partial t} + (u_j - \omega_j \eta)\frac{\partial \eta}{\partial x} + w_j \frac{\partial \eta}{\partial z} = v_j, \quad \text{on } y = \eta, \tag{1.2a}$$

$$q_2 - q_1 = g(\rho_2 - \rho_1)\,\eta, \qquad \text{on } y = \eta, \tag{1.2b}$$

while at the rigid boundaries

$$\left.\begin{aligned} v_1 &= 0, \quad \text{on } y = d_1, \\ v_2 &= 0, \quad \text{on } y = -d_2. \end{aligned}\right\} \tag{1.3}$$

We note that (1.1) and (1.2*a*, *b*) possess symmetry when $\omega_j \to -\omega_j$, $u_j \to -u_j$ and $x \to -x$. For a two-space-dimensional flow (i.e. one-dimensional in the propagation space) we put $w_j = 0$, and $\partial/\partial z = 0$. It may then be shown that vorticity is preserved, and assuming that the perturbed flow introduces no new vorticity, we can assume that the flow in each fluid is irrotational and described by a velocity potential ϕ_j and a stream function ψ_j, where

$$\boldsymbol{u}_j = \left(\frac{\partial \phi_j}{\partial x}, \frac{\partial \phi_j}{\partial y}, 0\right) = \left(\frac{\partial \psi_j}{\partial y}, -\frac{\partial \psi_j}{\partial x}, 0\right), \quad j = 1, 2. \tag{1.4}$$

Here both ϕ_j and ψ_j satisfy the two space-dimensional Laplace's equation. The reduced pressure is given by the Bernoulli relation

$$\frac{1}{\rho_j} q_j + \frac{\partial \phi_j}{\partial t} + \tfrac{1}{2}(u_j^2 + v_j^2) + \omega_j \psi_j - \omega_j y u_j = 0, \quad j = 1, 2. \tag{1.5}$$

Much of the discussion that follows is presented in dimensionless variables based on the lengthscale $2/k_0$ and the timescale $(2/k_0 \alpha g)^{\frac{1}{2}}$, where $\alpha = (\rho_2 - \rho_1)/(\rho_2 + \rho_1)$ is the Boussinesq parameter, and we recall that k_0 is the wavenumber of the basic wave. As far as possible we shall use the notation used in I and II. Thus, the dimensionless forms of $(x, y, z, t, p, q, \Delta, d_1, d_2, \omega_1, \omega_2)$ are $(X, Y, Z, T, P, Q, \delta, D_1, D_2, \Omega_2, \Omega_2)$, where 2Δ is the crest-to-trough amplitude of the basic wave. Note, in particular, that $P, Q)$ are the dimensionless forms of the modulation wavenumbers (p, q).

In §2 we consider resonant interactions of order N for infinitesimal waves in the

two-dimensional propagation space (i.e. the (P, Q)-plane). The main purpose of this is to determine the sites for resonant instability. One interesting feature that emerges is the existence for $Q \neq 0$ of an $N = 1$ resonance for sufficiently large values of the basic current shear, whereas it was shown in II that the lowest-order resonance is $N = 2$ in the absence of basic current shear (i.e. $\Omega_1 = \Omega_2 = 0$). In the Appendix we discuss the generic interaction equations for the $N = 1$ and $N = 2$ resonances in order to demonstrate the typical structure of the instability bands associated with these resonances. In §3 we consider the one-dimensional modulational instability theory, analogous to that developed in I. This theory provides information about instabilities when $Q = 0$, $P \ll 1$ and $\delta \ll 1$. The analytical results presented in §§2 and 3 are generally valid for the whole range of the parameter space defined by α, D_1, D_2, Ω_1 and Ω_2, but the specific examples discussed are largely motivated by the oceanic, or atmospheric, internal-wave application for which we put $\alpha = 0$, $D_2 \to \infty$, $\Omega_2 = 0$ and consider a range of values of D_1 and Ω_1. We also comment briefly on the application of our results to the air–water interface for which we put $\alpha = 0.9976$ and let $D_1, D_2 \to \infty$. Our numerical results for the finite-amplitude basic wave reported in Pullin & Grimshaw (1983*b*) are confined to the parameter values $\alpha = 0$, $D_2 \to \infty$, $\Omega_2 = 0$ for a range of values of D_1 and Ω_1, corresponding to the oceanic and atmospheric internal-wave applications. Consequently our numerical results for the instability of finite-amplitude waves, presented in §§4 and 5, are restricted to the same parameter values. We note that the corresponding numerical study of the instability of finite-amplitude waves at an air–water interface, possibly in the presence of basic current shear, would first require a calculation of the finite-amplitude basic wave states, which, to our knowledge, has not yet been carried out. In §4 the numerical technique is discussed briefly, as it is similar to that used in II, and is based on the method developed by McLean *et al.* (1981) and McLean (1982*a*, *b*) for the instability of water waves, and was also used by Yuen (1983) for interfacial waves. As in II, we find this numerical method provides results for wave stability when the basic wave amplitude lies in the range $0 < \delta < \max(\delta)$. In II we found that the limiting amplitude $\max(\delta)$ was determined by the onset of a local wave-induced K–H instability. That remains true here for small values of the basic current shear, but we also find that $\max(\delta)$ is determined by very slow convergence of the numerical scheme which is possibly associated with the development of a singularity in the perturbation. In §5 we present our numerical results for the one-dimensional instabilities ($Q = 0$) corresponding to the $N = 2$ resonance. For small values of the basic current shear the results are generally similar to those of II. However, as the basic current shear is increased some new effects appear. In particular one branch of the $N = 2$ instability band stabilizes for sufficiently large values of $-\Omega_1$, and we conjecture that this may be due to the influence of an $N = 1$ resonance, which, while always transverse ($Q \neq 0$), for large values of $-\Omega_1$ approaches the P-axis. Some analysis supporting this conjecture is discussed in the Appendix .

2. Two-dimensional resonant interactions

For small or moderate basic wave amplitudes we expect instability to be associated with a set of low-order resonances. This has been demonstrated for surface gravity waves by McLean *et al.* (1981) and McLean (1982*a*, *b*), and for interfacial waves in the absence of basic current shear ($\omega_1 = \omega_2 = 0$) by Yuen (1983) and in II. The resonances are defined in terms of the dispersion relation for infinitesimal waves of wavenumber $\boldsymbol{k} = (k, l)$ and frequency σ corresponding to solutions of the linearized

version of (1.1), (1.2a, b) and (1.3) in which η is given by an expression proportional to $\mathrm{Re}\{\exp(ikx+ilz-i\sigma t)\}$. We find that

$$\sigma^{\pm}(\boldsymbol{k}) = -\frac{\omega k}{4h\kappa} \pm \operatorname{sign} k \left\{ \frac{\omega^2 k^2}{16h^2\kappa^2} + \frac{g'\kappa}{h} \right\}^{\frac{1}{2}}, \tag{2.1a}$$

where

$$\omega = \frac{2(\rho_1\omega_1 - \rho_2\omega_2)}{\rho_1+\rho_2}, \tag{2.1b}$$

$$g' = \frac{g(\rho_2-\rho_1)}{\rho_2+\rho_1}, \quad h = \frac{(\rho_1 S_1 + \rho_2 S_2)}{\rho_1+\rho_2}, \tag{2.1c,d}$$

$$S_i = \coth \kappa d_i, \quad i = 1, 2 \quad \text{and} \quad \kappa = (k^2+l^2)^{\frac{1}{2}}. \tag{2.1e,f}$$

The superscript '$\pm$' indicates the presence of two branches of the dispersion relation, and will be omitted when both branches are being discussed. The sign convention in (2.1 a) is to ensure that $\sigma(\boldsymbol{k}) = -\sigma(-\boldsymbol{k})$. For real $\boldsymbol{k}$, $\sigma(\boldsymbol{k})$ is real-valued and hence the basic current shear is stable to infinitesimal perturbations. We also note that $\sigma^{\pm}(\boldsymbol{k};\omega) = -\sigma^{\mp}(\boldsymbol{k};-\omega)$ with the consequence that for the basic wave it will be sufficient to consider just the upper branch $\sigma^{+}(\boldsymbol{k},\omega)$ with ω taking both positive and negative values. Thus the 'lower-branch' infinitesimal and finite-amplitude steady wave solutions with $\omega < 0$, discussed in Pullin & Grimshaw (1983b) are considered here as σ^{+} solutions with $\omega > 0$.

Let us now suppose that the basic wave is propagating in the x-direction with a wavenumber $\boldsymbol{k}_0 = (k_0, 0)$ and frequency $\sigma_0 = \sigma^{+}(\boldsymbol{k}_0)$. This wave is then unstable owing to a resonant interaction with two other waves with wavenumbers $\boldsymbol{k}_1$ and $\boldsymbol{k}_2$ and frequencies, $\sigma_1 = \sigma(\boldsymbol{k}_1)$ and $\sigma_2 = \sigma(\boldsymbol{k}_2)$ whenever

$$\boldsymbol{k}_2 - \boldsymbol{k}_1 = N\boldsymbol{k}_0, \quad \sigma_2 - \sigma_1 = N\sigma_0. \tag{2.2}$$

Here N is a positive integer and defines the order of the resonance. We expect the growth rates of the instability to be $O(\delta^N)$ where δ is the wave steepness for the basic wave. In the Appendix we present the generic equations describing the $N = 1$ and $N = 2$ resonances, and indicate how the growth rates and bandwidth of the instabilities could be determined. The wavenumber resonance condition can be met by choosing $\boldsymbol{k}_1 = (p+nk_0, q)$, and $\boldsymbol{k}_2 = (p+nk_0+Nk_0, q)$. Here $\boldsymbol{p} = (p, q)$ can be regarded as the modulation wavenumber of the instability and the resonance condition (2.2) determines a curve in the (p, q)-plane. Relative to the modulation, the instability is n-periodic with respect to the basic wave, where n is an integer. Note that there is a degeneracy in the choice of p since the instability depends only on the combination $(p+nk_0)$. However, the resonance curves are symmetrical about $p = -nk_0 - \frac{1}{2}Nk_0$, $q = 0$, and following McLean (1982a, b) we remove the degeneracy by choosing $n = -\frac{1}{2}N$ for even N, and $n = -\frac{1}{2}(N+1)$ for odd N. With this choice the resonance curves are symmetrical about $p = 0$, $q = 0$ for even N, and $p = \frac{1}{2}k_0$, $q = 0$ for odd N. In the subsequent discussion it is useful to distinguish between a one-dimensional resonance when $q = 0$, and a two-dimensional or transverse resonance when $q \neq 0$, where we take the dimension to refer to the propagation space, rather than the physical space of the disturbance. All our results obtained from the modulational instability theory (see §3) or the numerical calculations (see §4) are for the one-dimensional case only. In order to facilitate comparison with the numerical calculations of §4, the resonance curves will be presented in non-dimensional form based on the lengthscale $2/k_0$ (or λ/π where λ is the wavelength of the basic wave) and the timescale $(2/k_0\alpha g)^{\frac{1}{2}}$ where $\alpha = (\rho_2-\rho_1)/(\rho_2+\rho_1)$ is the Boussinesq parameter

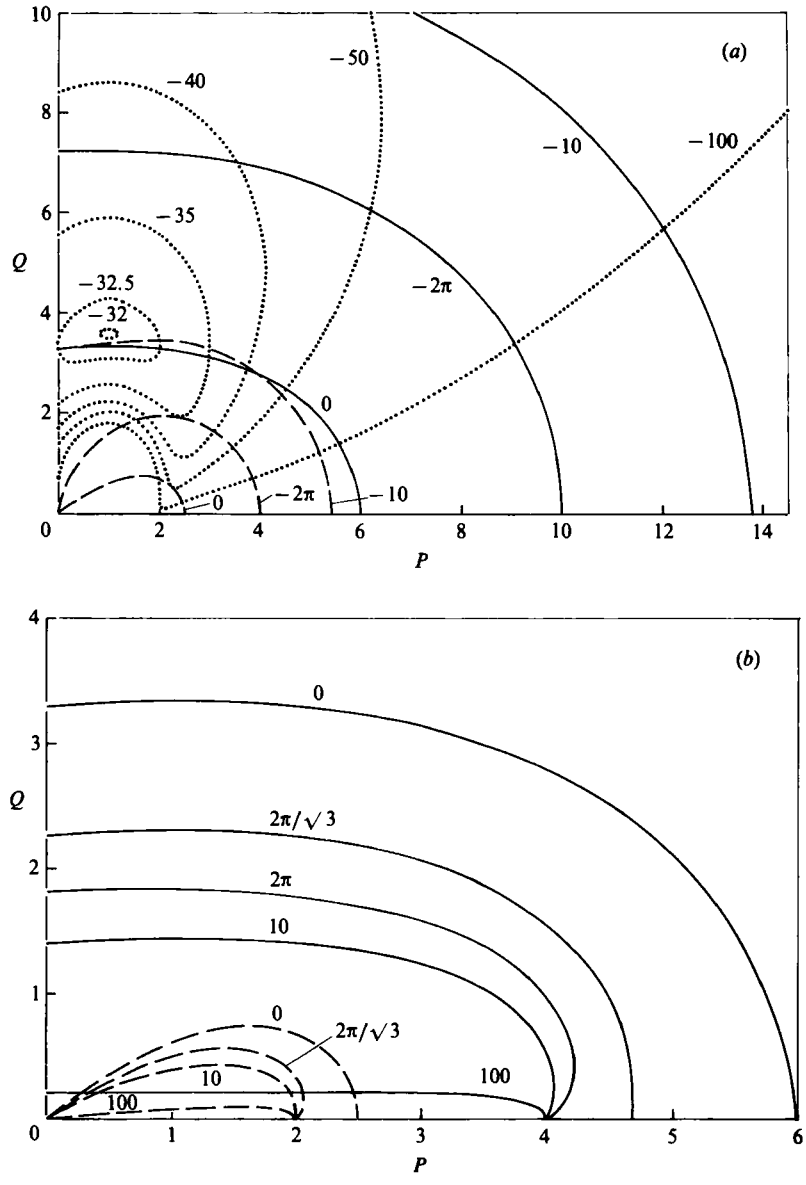

FIGURE 2. (*a*) Resonance curves for $H = 1$, $\Omega < 0$. Two different realizations are (i) D_1, $D_2 \to \infty$, $\alpha \to 0$, $\Omega_2 = 0$, $\Omega = \Omega_1$, (ii) D_1, $D_2 \to \infty$, $\alpha \to 1$, $\Omega = -2\Omega_2$. (*b*) Resonance curves for $H = 1$, $\Omega > 0$: no $N = 1$ resonances detected. ·····, $N = 1$; – – – –, $N = 2$; ——, $N = 3$. Values of $\pi\Omega$ shown.

and the Boussinesq limit is $\alpha \to 0$. The dimensionless parameters are now $D_{1,2} = \frac{1}{2}k_0 d_{1,2}$, $\Omega_{1,2} = (2/k_0 \alpha g)^{\frac{1}{2}} \omega_{1,2}$, $P = 2p/k_0$, $Q = 2q/k_0$ and α. Equations (2.1*b*, *d*) become respectively $\Omega = (1-\alpha)\Omega_1 - (1+\alpha)\Omega_2$ and $H = \frac{1}{2}\{(1-\alpha)S_1 + (1+\alpha)S_2\}$, where Ω and H are the dimensionless forms of ω and h. The resonance curves in the (P, Q)-plane are functions only of Ω and H, and do not depend explicitly on α.

The lowest-order resonance is $N = 1$ and corresponds to a triad interaction. It is readily shown that there are no one-dimensional resonances. Nor are there any transverse resonances in the absence of basic current shear ($\Omega_1 = \Omega_2 = 0$). However,

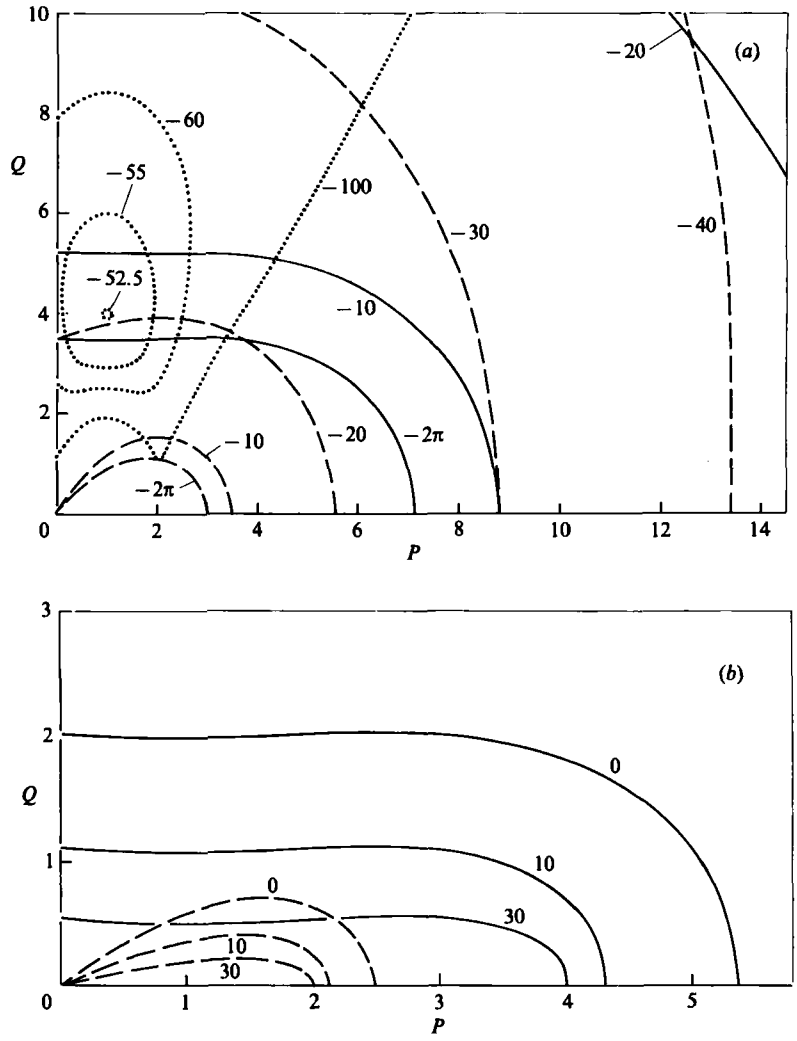

FIGURE 3. (*a*) Resonance curves for $H = 1.40$, $\Omega < 0$. One realization is $D_1 = 0.1\pi$, $D_2 \to \infty$, $\alpha \to 0$, $\Omega_2 = 0$, $\Omega = \Omega_1$. (*b*) Resonance curves for $H = 1.40$, $\Omega > 0$: no $N = 1$ resonances detected. Values of $\pi\Omega$ shown. For key see figure 2.

for sufficiently large negative values of Ω a transverse triad resonance exists. Some typical resonance curves are shown in figures 2 and 3. In figure 2 we show results when $D_1, D_2 \to \infty$. In this limit $H \to 1$ and the resonance curves are functions only of the single parameter Ω. The transverse triad resonance occurs for $\Omega < -10.196$, and at first appears as a small oval about the point $P = 1$, $Q = 3.5956$. As $|\Omega|$ increases the oval expands, and approaches the P-axis near the point $P = 2$. When either of D_1, D_2 is finite, the resonance curves are functions of both Ω and H. To provide a comparison with the numerical results of § 4 we show in figure 3 resonance curves for the case $H = 1.4$ as a function of Ω, corresponding in one realization to $D_1 = 0.1\pi$, $D_2 \to \infty$, in the Boussinesq approximation $\alpha = 0$. The resonance curves are generally similar to those in figure 2, although the critical value of $-\Omega$ for the appearance of the triad resonance is increased, and the resonance curves are displaced

further from the P-axis. It is useful to estimate the dimensional basic velocity shear that would be required to generate a triad resonance in an oceanic environment. Taking a typical wavelength of 500 m for an interfacial wave, $\alpha = 10^{-3}$ and $\Omega_1 \approx -52.5/\pi$ from figure 3(a), we find that the dimensional upper layer shear is $\omega_1 = 0.13\ \mathrm{s}^{-1}$. The required basic fluid velocity at $y = 50$ m is 6.6 m s^{-1}, which, while not totally unrealistic, is rather larger than a typical observation. At the other extreme, consider an air–water interface with basic velocity shear in the lower layer. With $D_1, D_2 \to \infty$, $\Omega_1 = 0$, $\alpha = 0.9976$ we find from figure 2(a) that $\Omega_2 \approx 16/\pi$ to generate a triad resonance. Taking a typical wavelength of 10 m for a surface gravity wave, we find that the dimensional lower-layer shear is $\omega_2 = 9.0\ \mathrm{s}^{-1}$, which is unrealistically large.

The next resonance is $N = 2$ and corresponds to a quartet interaction. This resonance exist for all values of the parameters Ω and H. In the absence of basic current shear (i.e. $\Omega = 0$) the resonance curve is a figure-of-eight, very similar to the resonance curve obtained for surface gravity waves (Phillips 1960). For small values of $|\Omega|$ the resonance curve remains a figure-of-eight, but for larger vales of $|\Omega|$ two new effects appear. We refer first to figure 2 where we show results for the case $D_1 D_2 \to \infty$ (i.e. $H \to 1$) when the resonance curves are functions of the single parameter Ω. First, for $\Omega < -2$ the resonance curves detach from the original and form ovals centred on the origin, although we note that the origin satisfies the resonance condition as an isolated point. Next, for $\Omega > 2/3^{\frac{1}{2}}$, the resonance curves all pass through the point $P = 2$, $Q = 0$, and the angle of contact with the P-axis at this point varies from 0 at $\Omega = 2/3^{\frac{1}{2}}$ to $\frac{1}{2}\pi$ as $\Omega \to \infty$. In figure 3, where we show the case $H = 1.4$ (corresponding to the realization $D_1 = 0.1\pi$, $D_2 \to \infty$, $\alpha = 0$), the resonance curves show similar behaviour, although a larger value of $-\Omega$ is required for the resonance curves to detach from the origin, and the limit point at $P = 2$, $Q = 0$ is only approached as $\Omega \to \infty$.

In the Appendix we have determined generic expressions for the growth rate and bandwidth of the $N = 2$ instability. In particular the instability band is defined by (see (A 10a))

$$\epsilon^2 G_- |A|^2 < G < \epsilon^2 G_+ |A|^2, \tag{2.3a}$$

where

$$2G = \sigma(\boldsymbol{k}_0 + \boldsymbol{p}) + \sigma(\boldsymbol{k}_0 - \boldsymbol{p}) - 2\sigma(\boldsymbol{k}_0). \tag{2.3b}$$

Here ϵA is the complex amplitude of the basic wave and $G_\pm$ are functions of $\boldsymbol{k}_0$, $\boldsymbol{p}$ and the basic-state parameters (here Ω_1, Ω_2, D_1, D_2 and α). G is a detuning parameter which vanishes when the exact resonance condition (2.2) is satisfied. In the Appendix we show that near the origin of the (p, q)-plane, the instability criterion for the $N = 2$ resonance reduces to that obtained from the long-wavelength modulational instability theory of small-amplitude waves. For the one-dimensional case ($q = 0$) this theory is presented in §3, and analytical expressions for bandwidth and growth rates found. Returning to (2.3a, b) for this one-dimensional case ($q = 0$), it is apparent from the resonance curves in figures 2 and 3 that there are two possible instability bands. One is located near the origin of the (P, Q)-plane, and the other on the P-axis in the region $P \geqslant 2$. Considering the band near the origin, it may be shown that $G < 0$. Then if $G_+ \geqslant 0$ a necessary condition for instability is that $G_- < 0$ and the instability band includes the point $P = 0$. But if $G_+ < 0$, the instability band detaches from the point $P = 0$. Our numerical results presented in §5 show evidence of both cases, the former occurring for smaller values of the basic current shear. We conclude this brief discussion by noting that although there are no triad resonances when $Q = 0$, the

triad resonance curves approach the P-axis near $P = 2$ for sufficiently large values of $-\Omega$ (see figures 2 and 3). In the Appendix we show that the proximity of a triad resonance to an $N = 2$ instability band may be stabilizing. Some evidence for this behaviour is presented from our numerical results in §5.

All the higher-order resonances $N \geqslant 3$ exist, and resonance curves for $N = 3$ are shown in figures 2 and 3. They are generally similar to those that occur in the absence of basic current shear ($\Omega = 0$) although we note that in figure 2 (D_1, $D_2 \to \infty$) all the resonance curves pass through the point $P = 4$, $Q = 0$ for $\Omega > 2$, and in figure 3 (D_1 finite, $D_2 \to \infty$) the resonance curves approach the point $P = 4$, $Q = 0$ as $\Omega \to \infty$.

3. One-dimensional modulational instability for small-amplitude waves

In §2 we noted that the origin, $p = q = 0$, is always a point (possibly isolated) on the $N = 2$ resonance curve. This implies the potential existence of a long-wavelength modulational instability for small-amplitude waves. The instability is best discussed within the context of the equations that describe slowly-modulated small-amplitude waves. For one-dimensional modulations (i.e. $q = 0$) the relevant equation is the nonlinear Schrödinger equation

$$\mathrm{i}\frac{\partial \eta_1}{\partial \tau} + \lambda \frac{\partial^2 \eta_1}{\partial \xi^2} + \nu |\eta_1|^2 \eta_1 = 0, \tag{3.1a}$$

where

$$\tau = \epsilon^2 t, \quad \xi = \epsilon(x - Vt). \tag{3.1b}$$

Here $\epsilon\eta_1$ is the complex wave amplitude, and to leading order the wave is described by $\epsilon\eta_1 \exp(\mathrm{i}k_0 x - \mathrm{i}\sigma_0 t)$, where $\sigma_0 = \sigma(k_0)$ (i.e. (2.1a) with $\boldsymbol{k} = (k_0, 0)$). The group velocity is $V = \partial\sigma/\partial k$ and the coefficient $\lambda = \frac{1}{2}\partial V/\partial k$, where both expressions are evaluated at $k = k_0$. The coefficient ν of the nonlinear term is determined by the interaction of the second harmonic and the wave-induced mean flow with the primary wave. The derivation of (3.1a), which we shall sketch below, requires that ϵ be a small parameter, and the equation describes a balance between nonlinearity and wave dispersion about the dominant wavenumber k_0. It is well known that the nonlinear Schrödinger equation (3.1a) is a generic equation describing undirectional wave modulation (see, for instance, Benney & Newell 1967), and in particular it has been shown to describe the modulation of surface gravity waves (Zakharov 1968). Equation (3.1a) has the plane-wave solution with constant amplitude A

$$\eta_1 = A \exp(\mathrm{i}\nu |A|^2 \tau). \tag{3.2}$$

When this is subjected to modulational perturbations with real and imaginary parts proportional to

$$\mathrm{Re}\{\exp(\hat{s}\tau + \mathrm{i}\hat{p}\xi)\}, \tag{3.3}$$

then there is modulational instability whenever $\lambda\nu > 0$ and the growth rate $\hat{s}$ is given by

$$\hat{s}^2 = \lambda \hat{p}^2(2\nu |A|^2 - \lambda \hat{p}^2). \tag{3.4}$$

There is instability for $0 < \hat{p}^2 < 2\nu\lambda^{-1}|A|^2$ with a maximum growth rate of $\nu|A|^2$ at $\lambda\hat{p}^2 = \nu|A|^2$. Note that the unscaled growth rate is $s = \epsilon^2\hat{s}$ and the unscaled modulation wavenumber is $p = \epsilon\hat{p}$.

In order to use (3.4) we must obtain an expression for the nonlinear coefficient ν.

In the absence of basic current shear ($\omega_1 = \omega_2 = 0$), we derived in I a two-dimensional nonlinear Schrödinger equation coupled to an equation describing the wave-induced mean flow, which reduced to the form (3.1 *a*) for one-dimensional modulations. However, the inclusion of basic current shear has the effect of introducing vorticity when two-dimensional modulations are considered, with the consequent presence of critical layers. This makes the derivation of equations describing two-dimensional modulations a difficult task, and since our numerical results in §4 are restricted to one-dimensional perturbations, for essentially the same reason, we shall consider only one-dimensional modulations here. In this case the perturbed flow is described by a velocity potential (see 1.4) and (1.5) and the derivation of (3.1 *a*) follows a similar course to that described in I. We shall give a brief outline, partly in order to develop notation.

We shall find it useful to develop the theory for the case when the basic flow in each layer is $\bar{u}_i - \omega_i y (i = 1, 2$, for the upper, lower layer respectively). Later we shall put $\bar{u}_1 = \bar{u}_2 = 0$. Modulated waves are described by

$$\eta = \sum_{-\infty}^{\infty} \epsilon^{|n|} \eta_n(\xi, \tau) \exp\left(\mathrm{i}n(k_0 x - \sigma_0 t)\right), \quad \eta_{-n} = \eta_n^* \tag{3.5}$$

with similar expressions for ϕ_i. Substitution into the equations of motion and boundary conditions then gives

$$\epsilon D(\hat{\sigma}, \hat{k})\, \eta_1 + N_1 = 0, \tag{3.6a}$$

where

$$\hat{\sigma} = \sigma_0 + \mathrm{i}\epsilon\left(-V\frac{\partial}{\partial \xi} + \epsilon\frac{\partial}{\partial \tau}\right), \quad \hat{k} = k_0 - \mathrm{i}\epsilon\frac{\partial}{\partial \xi}, \tag{3.6b}$$

and

$$D(\sigma, k) = (\rho_2 - \rho_1) g - \rho_2 \frac{(\sigma - k\bar{u}_2)^2}{k} S_2 - \rho_1 \frac{(\sigma - k\bar{u}_1)^2}{k} S_1 + \rho_2 \omega_2 \frac{(\sigma - k\bar{u}_2)}{k} - \rho_1 \omega_1 \frac{(\sigma - k\bar{u}_1)}{k}, \tag{3.6c}$$

where henceforth $S_i = \coth k d_i$, Note that $D(\sigma, k) = 0$ generates the dispersion relation (2.1 *a*) (with $l = 0$). Here N_1 represents nonlinear terms, and to $O(\epsilon^3)$ is given by

$$N_1 = \epsilon^3 (\nu_0 + \nu_2) |\eta_1|^2 \eta_1, \tag{3.7}$$

where ν_0 and ν_2 correspond to terms arising from the interaction of the primary wave with the wave-induced mean flow and the second harmonic respectively. We find that

$$\nu_0 = -\frac{I_0^2}{D_0} - \frac{1}{\rho_1 d_1}\left(\frac{\partial D}{\partial \bar{u}_1}\right)^2 - \frac{1}{\rho_2 d_2}\left(\frac{\partial D}{\partial \bar{u}_2}\right)^2, \tag{3.8a}$$

where

$$I_0 = -\left(\frac{\partial D}{\partial d_2} - \frac{\partial D}{\partial d_1}\right) + \frac{(\bar{u}_2 - V + d_2 \omega_2)}{d_2}\frac{\partial D}{\partial \bar{u}_2} - \frac{(\bar{u}_1 - V - d_1 \omega_1)}{d_1}\frac{\partial D}{\partial \bar{u}_1}, \tag{3.8b}$$

and

$$D_0 = (\rho_2 - \rho_1) g - \frac{\rho_2}{d_2}(\bar{u}_2 - V)^2 - \frac{\rho_1}{d_1}(\bar{u}_1 - V)^2 - \rho_2 \omega_2 (\bar{u}_2 - V) + \rho_1 \omega_1 (\bar{u}_1 - V). \tag{3.8c}$$

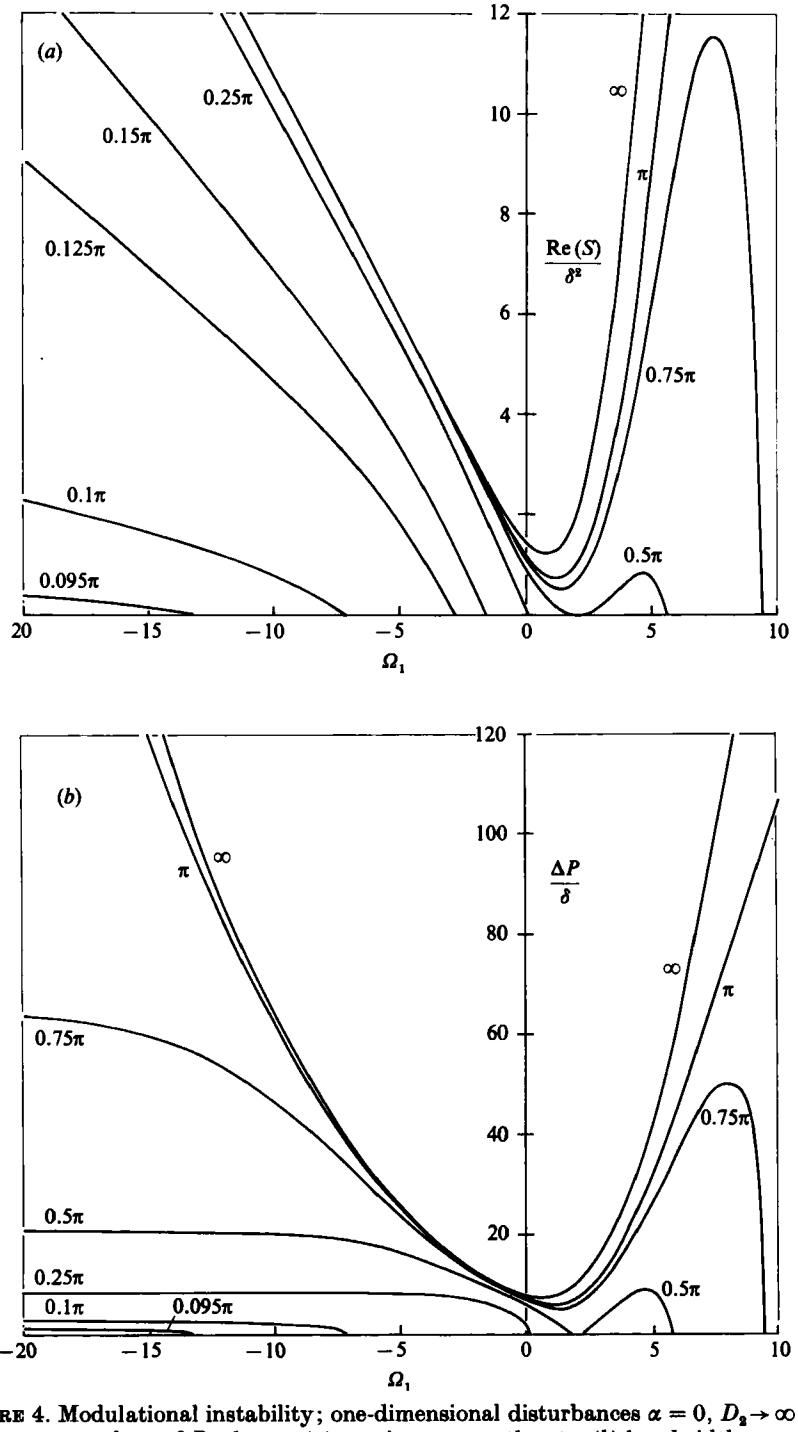

FIGURE 4. Modulational instability; one-dimensional disturbances $\alpha = 0$, $D_2 \to \infty$, $\Omega_2 = 0$, values of D_1 shown. (*a*) maximum growth rate, (*b*) bandwidth.

Note that D_0 is the limit as $k \to 0$ of $D_0(kV, k)$ and does not vanish when $\bar{u}_1 = \bar{u}_2 = 0$ (i.e. there is no long-wave resonance). Next

$$\begin{aligned} k_0^{-3}\nu_2 = {} & \tfrac{1}{2}[\rho_2(c-\bar{u}_2)^2(3S_2^2-1) - \rho_1(c-\bar{u}_1)^2(3S_1^2-1) \\ & - \rho_1\hat{\omega}_1\{(c-\bar{u}_1)(3S_1+S_1^{-1}) + \hat{\omega}_1\} - \rho_2\hat{\omega}_2\{(c-\bar{u}_2)(3S_2+S_2^{-1}) - \hat{\omega}_2\}] \\ & \times [\rho_2 S_2^{-1}(c-\bar{u}_2)^2 + \rho_1 S_1^{-1}(c-\bar{u}_1)^2]^{-1} - 2\rho_2(c-\bar{u}_2)^2 S_2(S_2^2-2) \\ & - 2\rho_1(c-\bar{u}_1)^2 S_1(S_1^2-2) + \rho_2\hat{\omega}_2\{2(c-\bar{u}_1)(S_1^2-1) - \tfrac{1}{2}\hat{\omega}_2(S_2+S_2^{-1})\} \\ & - \rho_1\hat{\omega}_1\{2(c-\bar{u}_2)(S_1^2-1) + \tfrac{1}{2}\hat{\omega}_1(S_1+S_1^{-1})\}, \end{aligned} \tag{3.9a}$$

where

$$c = \frac{\sigma_0}{k_0}, \quad \hat{\omega}_1 = \omega_i k_0^{-1} \quad \text{for } i = 1, 2. \tag{3.9b}$$

Expanding (3.6*b*) to $O(\epsilon^3)$ we obtain (3.1*a*) with

$$D_\sigma \nu = \nu_0 + \nu_2. \tag{3.10}$$

Henceforth, we put $\bar{u}_1 = \bar{u}_2 = 0$. It is then readily shown that $\lambda < 0$ and hence for instability to occur we must have $\nu < 0$. Since $D_\sigma < 0$ instability requires that $(\nu_0 + \nu_2) > 0$. But from (3.8*a*) $\nu_0 < 0$ and hence the interaction of the primary wave with the wave-induced mean flow is stabilizing and instability requires that ν_2 be sufficiently negative. In presenting our results we again use non-dimensional coordinates based on the lengthscale $2/k_0$ and the timescale $(2/k_0\alpha g)^{\frac{1}{2}}$ where we recall that $\alpha = (\rho_2 - \rho_1)/(\rho_2 + \rho_1)$ is the Boussinesq parameter. The dimensionless parameters are $D_{1,2} = \frac{1}{2}k_0 d_{1,2}$, $\Omega_{1,2} = (2/k_0\alpha g)^{\frac{1}{2}}\omega_{1,2}$ and α. The non-dimensional modulation wavenumber is $P = 2\epsilon\hat{p}/k_0$ and the non-dimensional growth rate is $S = \epsilon^2\hat{s}(k_0\alpha g/2)$. Further it is apparent from (3.4) that P scales with the non-dimensional amplitude $\delta = \epsilon k_0|A|$ and the growth rate S scales with δ^2. Hence our results are expressed in units of $P\delta^{-1}$ and $S\delta^{-2}$.

In general the coefficients ν and λ are complicated functions of the parameters D_1, D_2, Ω_1, Ω_2, and α, and hence we have evaluated them numerically. All our results are for an upper-branch basic wave (i.e. $\sigma_0 = \sigma^+(k_0)$ in (2.1*a*)). Some typical results are shown in figures 4, 5 and 6 for the growth rate and bandwidth of the modulational instability deduced from (3.4). It is apparent that basic current shear, represented by the parameters Ω_1 and Ω_2, can in some circumstances dramatically increase the growth rate of the instability, and in other circumstances remove the instability altogether. For simplicity let us consider the case of infinitely deep fluid on both sides of the interface, i.e. D_1, $D_2 \to \infty$, and note that for the finite values of D_1 or D_2 shown the results are generally similar but with reduced growth rates. When D_1, $D_2 \to \infty$, ν and λ are functions of just three parameters Ω_1, Ω_2 and α and some analysis is possible.

Consider first the case $\Omega_2 = 0$, when the basic current shear is confined to the upper fluid. In figure 4 we show the case $\alpha \approx 0$, which we remind the reader corresponds to potential oceanic or atmospheric applications. There is instability for nearly all values of Ω_1, with the growth rates generally increasing as $|\Omega_1|$ increases. However, as $\Omega_1 \to -\infty$ there exists a critical value $\Omega_{1c}^- \approx -2^{\frac{3}{2}}\alpha^{-1}$ such that for $\Omega < \Omega_1$ there is modulational stability. The dimensional value of Ω_{1c}^- is $\omega_{1c}^- \approx -2(k_0 g/\alpha)^{\frac{1}{2}}$. As α increases there is modulational stability for $\Omega < \Omega_{1c}^- < 0$, where Ω_{1c}^- at first increases with α, but then decreases; as $\alpha \to 1$, $\Omega_{1c}^- \approx -2.12(1-\alpha)^{-\frac{1}{4}}$. For $0.347 < \alpha < 0.5$ there is also modulational stability for $0 < \Omega_{1c}^+ < \Omega_1 < \Omega_{1c}^{++}$; as $\alpha \to 0.5$, $\Omega_{1c}^{++} \simeq \infty$ and for $\alpha > 0.5$ there is modulational stability for $\Omega > \Omega_{1c}^+$ where $\Omega_{1c}^+ \approx 2.12(1-\alpha)^{-\frac{1}{4}}$

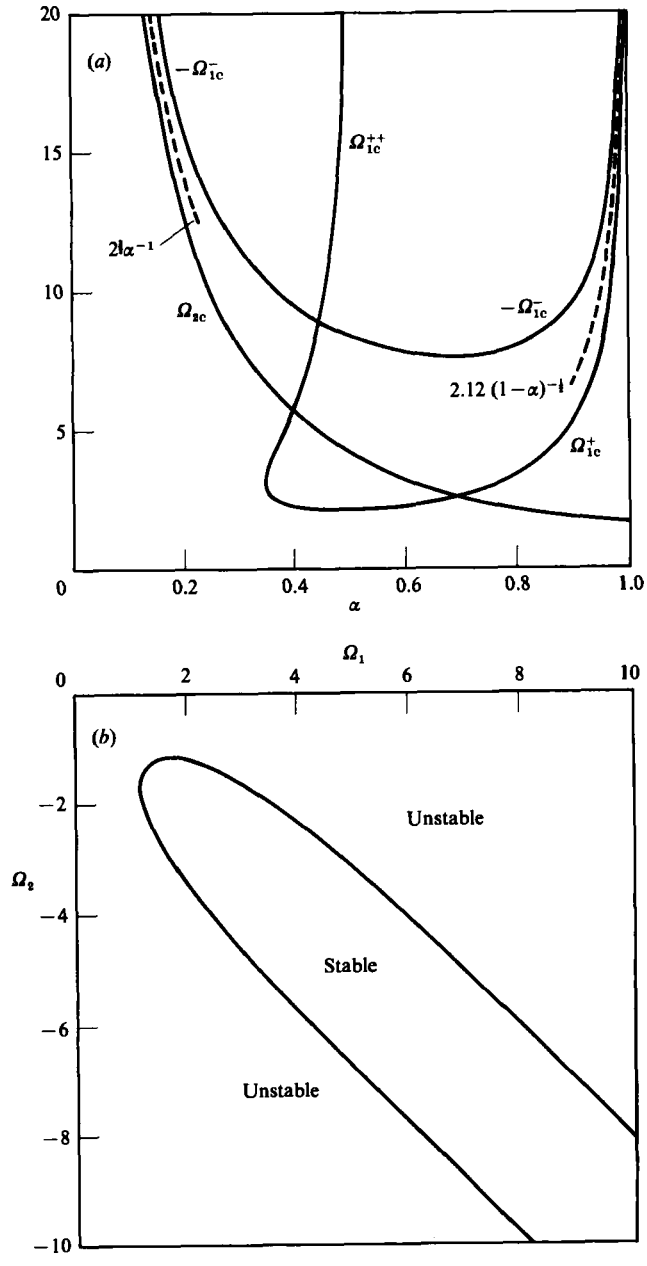

FIGURE 5. (*a*) Cutoff parameters Ω_{1c}^{-}, Ω_{1c}^{+} and Ω_{1c}^{++} for modulational instability D_1, $D_2 \to \infty$, $\Omega_2 = 0$. Also Ω_{2c} for $\Omega_1 = 0$. (*b*) Modulational instability boundary in fourth quadrant of (Ω_1, Ω_2)-plane, D_1, $D_2 \to \infty$, $\alpha = 0$.

as $\alpha \to 1$. The variation of these boundaries with α is shown in figure 5(*a*). The case $\alpha \approx 1$ is shown in figure 6, where the value of α corresponds to an air–water interface, and shows that basic current shear in the air reduces the growth rate of the modulational instability of deep-water surface gravity waves.

Next, we again let D_1, $D_2 \to \infty$, and put $\Omega_1 = 0$, so that the basic current shear is confined to the lower fluid. There is modulational stability for $\Omega_2 > \Omega_{2c} > 0$ where

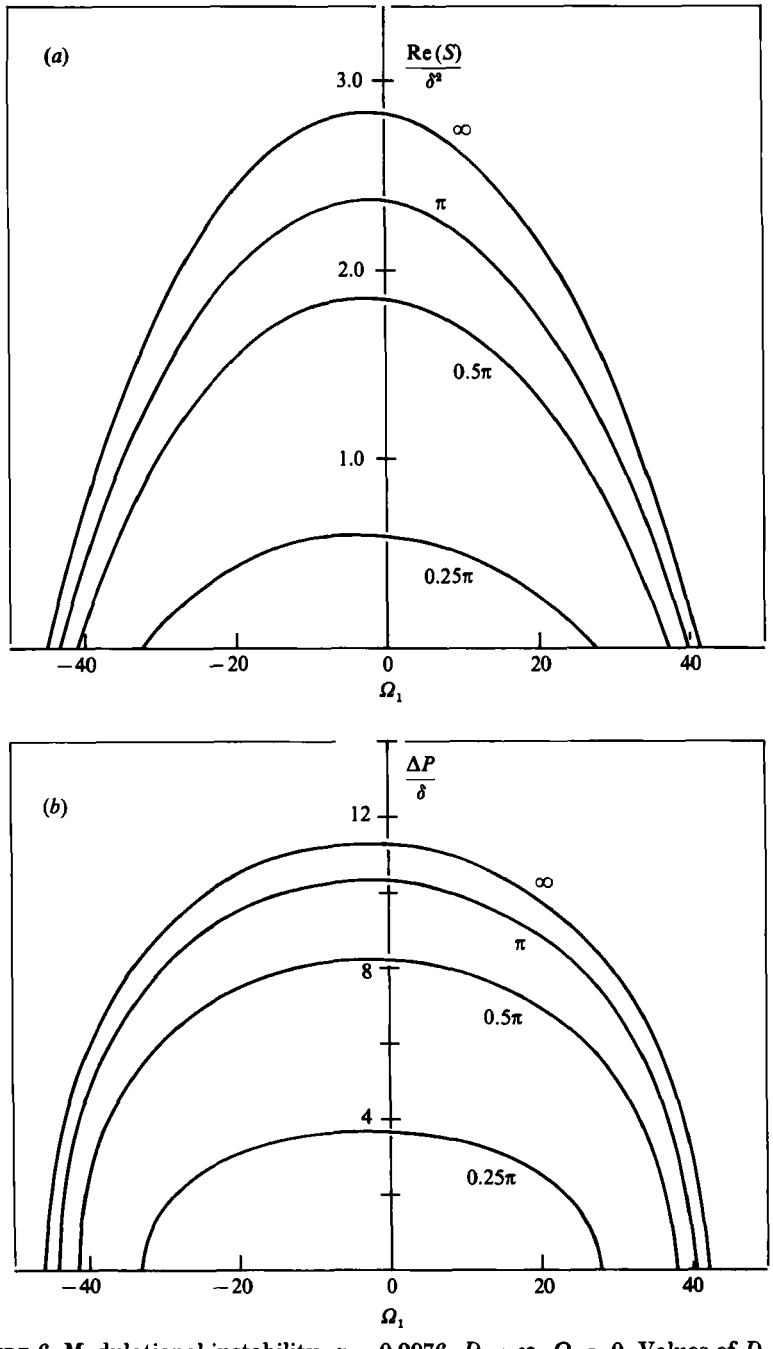

FIGURE 6. Modulational instability. $\alpha = 0.9976$, $D_1 \to \infty$, $\Omega_2 = 0$. Values of D_2 shown. (a) maximum growth rate, (b) bandwidth.

$\Omega_{2c} \approx 2^{\frac{1}{2}}\alpha^{-1}$ as $\alpha \to 0$ (the corresponding dimensional value is $\omega_{1c} \approx 2(k_0 g/\alpha)^{\frac{1}{2}}$) and Ω_{2c} decreases to $\frac{2}{3}\sqrt{6} \approx 1.633$ as $\alpha \to 1$. The variation of Ω_{2c} with α is shown in figure 5(a). The case $\alpha \approx 1$ is shown in figure 7, where the value of α corresponds to an air–water interface, and shows that sufficiently large positive basic current shear in the water eliminates the modulational instability of deep-water surface gravity waves, but that negative basic current shear increases the growth rate.

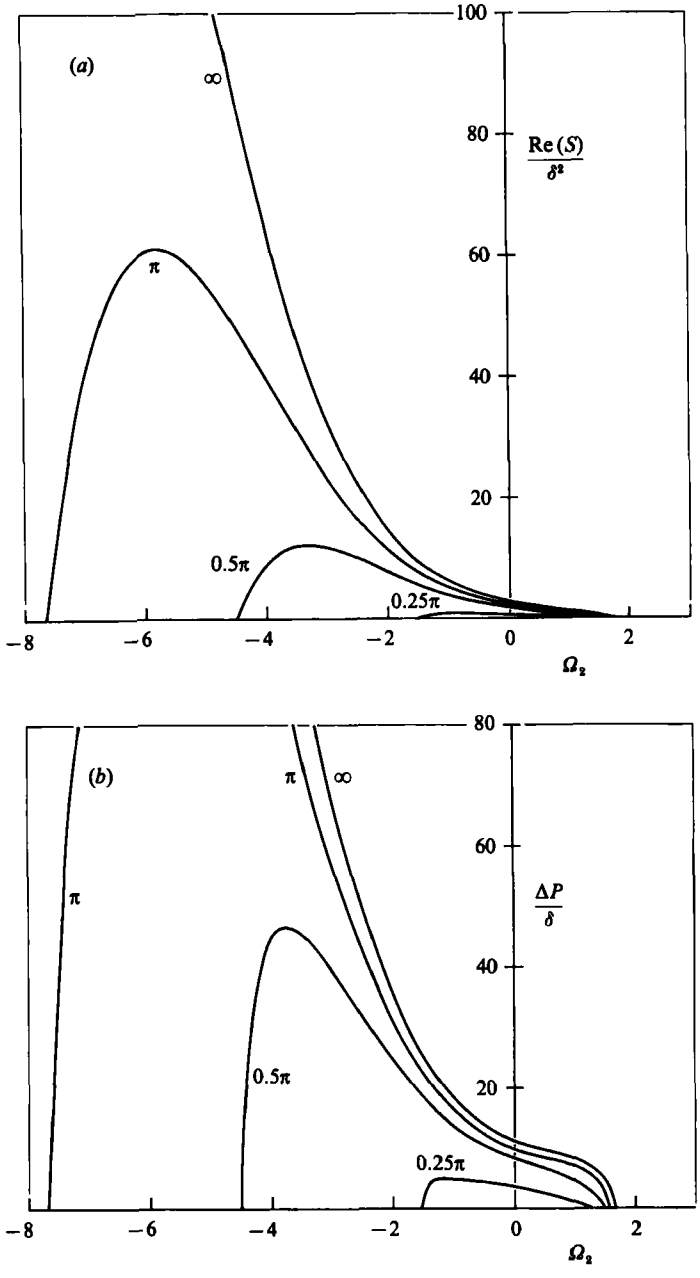

FIGURE 7. (*a*) Maximum growth rate of modulational instability: $\alpha = 0.9976$, $D_1 \to \infty$. $\Omega_1 = 0$. (*b*) Bandwidth of modulational instability: $\alpha = 0.9976$, $D_1 \to \infty$, $\Omega_1 = 0$. Values of D_2 shown.

Finally in the Boussinesq limit $\alpha \to 0$, ν and λ are functions of Ω_1, Ω_2. It can be shown that there is modulational instability for all values of Ω_1, Ω_2 except for a certain region in the fourth quadrant of the (Ω_1, Ω_2)-plane (see figure 5*b*). It should be noted here that the limits $\alpha \to 0$ and either $|\Omega_1| \to \infty$ or $|\Omega_2| \to \infty$ do not necessarily commute.

4. Numerical analysis for one-dimensional instability

Here we present numerical calculations of the one-dimensional linearized instability of the basic wave for finite values of the basic wave amplitude δ and finite values of the modulation wavenumber P, thus complementing the analytical results of §3. The basic flow consists of the basic current shear (see figure 1), together with the finite-amplitude progressive interfacial waves described both analytically and numerically in Pullin & Grimshaw (1983*b*). In dimensionless variables the basic wave has crest-to-trough amplitude 2δ, and is periodic in the X-direction with period π. The numerical solutions for the basic wave were confined to the parameter space $\alpha = 0$, $D_2 \to \infty, 0 < D_1 < \infty, \Omega_2 = 0$, $|\Omega_1| \geqslant 0$ (motivated by potential oceanic or atmospheric applications) and $0 < \delta < \delta_{\max}$, where $\delta_{\max}$ corresponds to the highest wave that could be found numerically.

Since three-space-dimensional perturbations are generally not vorticity-preserving, we shall restrict our attention to two-space-dimensional perturbations (i.e. one-dimensional in the propagation space), for which we may assume that the perturbed flow is irrotational. In the terminology of §2 our numerical results are thus restricted to the case when the modulation wavenumber is one-dimensional (i.e. $Q = 0$). The important case of two-dimensional, or transverse, instability (i.e. $Q \neq 0$) cannot be formulated within the framework of irrotational flow, and awaits further study. We also note that there may be one-dimensional instabilities corresponding to a two-space-dimensional perturbations which perturb the vorticity field, but since these also cannot be described by irrotational disturbances to the basic wave, they are not considered here.

The numerical method used is a straightforward extension of that developed by McLean *et al.* (1981) and McLean (1982*a*, *b*) for the instability of water waves, and utilized by Yuen (1983), and in II, for interfacial waves in the absence of basic current shear. Hence we shall give only a brief outline of its salient features. We choose a frame of reference at rest with respect to the steady progressive wave. Using non-dimensional variables and the Boussinesq approximation $\alpha \to 0$, the boundary conditions can be obtained from (1.2*a*, *b*) and (1.5) and are

$$\frac{\partial \eta}{\partial T} + (U_j - \Omega_j \eta)\frac{\partial \eta}{\partial X} = V_j, \quad j = 1, 2, \quad \text{on } Y = \eta, \tag{4.1a, b}$$

and

$$\frac{\partial \Phi_2}{\partial T} - \frac{\partial \Phi_1}{\partial T} + \tfrac{1}{2}\{(U_2 - \Omega_2 \eta)^2 + V_2^2 - (U_1 - \Omega_1 \eta)^2 - V_1^2\} - \Omega_2(\Psi_2 - \tfrac{1}{2}\Omega_2 \eta^2) - \Omega_1(\Psi_1 - \tfrac{1}{2}\Omega_1 \eta^2) + 2\eta = 0, \quad \text{on } Y = \eta. \tag{4.1c}$$

Next we let $\Omega_2 = 0$, $D_2 \to \infty$ and put

$$\eta = \bar{\eta}(X) + \eta'(X, T), \tag{4.2a}$$

$$\Phi_j = \bar{\Phi}_j(X, Y) + \phi_j'(X, Y, T), \quad j = 1, 2 \tag{4.2b}$$

$$\Psi_1 = \bar{\Psi}_1(X, Y) + \psi_1'(X\ Y, T), \tag{4.2c}$$

where $\bar{\eta}$, $\bar{\Phi}_j$ and Ψ_1 are the solutions for the steady finite-amplitude basic wave, and η', ϕ_j' and ψ_1' are the small perturbations. Substituting (4.2*a*, *b*, *c*) into (4.1*a*, *b*, *c*) and linearizing about the basic wave solution gives a set of boundary conditions evaluated on $Y = \bar{\eta}_1(X)$ which are linear in η', ϕ_j' and ψ_1'. Noting that ϕ_j' and ψ_1'

satisfy Laplace's equation, and using the boundary conditions at $Y = D_1$ and as $Y \to -\infty$, we seek solutions of the form

$$\eta' = \exp(ST + \mathrm{i}PX) \sum_{-\infty}^{\infty} a_m \exp(2\mathrm{i}mX), \tag{4.3a}$$

$$\phi_1' = \exp(ST + \mathrm{i}PX) \sum_{-\infty}^{\infty} b_m \exp(2\mathrm{i}mX) \frac{\cosh[R_m(D_1 - Y)]}{\cosh[R_m D_1]}, \tag{4.3b}$$

$$\psi_1' = -\mathrm{i}\exp(ST + \mathrm{i}PX) \sum_{-\infty}^{\infty} \hat{b}_m \exp(2\mathrm{i}mX) \frac{\sinh[R_m(D_1 - Y)]}{\cosh[R_m D_1]}, \tag{4.3c}$$

$$\phi_2' = \exp(ST + \mathrm{i}PX) \sum_{-\infty}^{\infty} c_m \exp(2\mathrm{i}mX) \exp[R_m Y], \tag{4.3d}$$

where $R_m = |2m + P|$, $\hat{b}_m = b_m \operatorname{sign}(2m + P)$, P is the modulation wavenumber and S is the growth rate. Substitution of (4.3*a–d*) into the linearized boundary conditions then gives an eigenvalue problem for the complex coefficients (a_m, b_m, c_m) and the eigenvalue S. Instability corresponds to $\mathrm{Re}(S) > 0$.

When $\delta = 0$, the solution is that for infinitesimal waves on the basic current shear (see figure 1). The eigenvalues are $S_n = -\mathrm{i}\hat{\sigma}_n^{\pm}$, where $\hat{\sigma}_n^{\pm}$ can be obtained from the dispersion relation (2.1*a*) with $\alpha = 0$, $\Omega_2 = 0$ and $D_2 \to \infty$. Thus we find that

$$\hat{\sigma}_n^{\pm} = C_0(P + 2n) + W^{\pm}(P + 2n), \tag{4.4a}$$

where

$$W^{\pm}(P) = \frac{\operatorname{sign}(P)[-\Omega_1 \pm \{\Omega_1^2 + 8|P|(1 + \coth|P| D_1)\}^{\frac{1}{2}}]}{[2(1 + \coth|P| D_1)]}, \tag{4.4b}$$

and C_0 is the phase speed of the basic wave, i.e. $C_0 = \frac{1}{2}W^{+}(2)$. If we put $k = P + 2n$, then $\hat{\sigma}_n^{\pm} = -C_0 k + W^{\pm}(k)$ and corresponds to the linear dispersion relation in a frame of reference moving with speed C_0. For small δ, instabilities occur whenever two of these linear modes satisfy the resonance condition

$$\hat{\sigma}_n(P) = \hat{\sigma}_{n+N}(P) \tag{4.5}$$

for specified P and some integers n, N. Here the superscripts '$\pm$' are omitted as both branches can participate in the condition (4.5). Identifying $k_1 = P + 2n$, $k_2 = P + 2n + 2N$ and $k_0 = 2$ it is readily seen that the resonance condition (4.5) is equivalent to (2.2), although here we are restricting attention to the one-dimensional case (i.e. $Q = 0$). In §2 we identified the resonance curves on which (2.2), or (4.5), is satisfied, and thus determined the values of modulation wavenumber P around which the instability bands will be located for small δ. We recall that for one-dimensional instabilities, the $N = 1$ resonance condition cannot be satisfied and the lowest-order resonance is $N = 2$.

When δ and P are both small, the modulational instability theory of §3 applies and describes the features of the one-dimensional instability corresponding to the $N = 2$ resonance for $\delta \approx 0$ near $P = 0$. For finite values of P, and for finite δ, the eigenvalue problem for S must be solved numerically. First, the infinite series in (4.3*a–d*) are truncated at $m = M$. The linearized boundary conditions are then satisfied at $2M + 1$ points on a single wavelength, $0 \leqslant X \leqslant \pi$, of the basic wave, with the various coefficients (which contain functions of $\bar{\eta}(X)$, $\bar{\Phi}_j(X, Y)$ and $\bar{\Psi}_1(X, Y)$ evaluated on $Y = \bar{\eta}(X)$) being calculated from the progressive wave solutions obtained by Pullin & Grimshaw (1983*b*). This procedure results in a discrete $(6M + 3) \times (6M + 3)$ eigenvalue problem with eigenvector $[a_{-M} \ldots a_M; b_{-M} \ldots b_M;$

$c_{-M} \ldots c_M]$, which can be solved numerically by codes based on the well-known QZ or LZ algorithms. As in II, the $(6M+3)\times(6M+3)$ system contains a $(2M+1)$-fold degeneracy due to overspecification of the boundary conditions on $Y = \bar{\eta}(X)$. This degeneracy can either be removed through contraction based on matrix implementation of the sufficient boundary conditions (see II), or the larger degenerate system can be handled directly, with some computational penalty. Both options were utilized, and comparisons between the respective results were used as one check on accuracy.

The calculations reported here were obtained in that portion of the basic wave parameter space defined by $D_1 \to \infty$. 0.5π and 0.1π, $-100/\pi \leqslant \Omega_1 < 5$ and for $\delta = 0.005\pi$, 0.01π, 0.025π and 0.05π. The truncation number M varied in the range $10 \leqslant M \leqslant 50$, and all computations were carried out in double precision (14 figure) arithmetic, using both VAX 11/780 and IBM 3083 machines. The values of δ used were always less than $\max(\delta)$ (a function of Ω_1 and D_1), which is that basic wave amplitude beyond which we could not obtain satisfactory convergence of the physically significant eigenvalues with increasing M. In II (i.e. $\Omega_1 = 0$) we found that $\max(\delta)$ was determined by the onset of a wave-induced local K–H instability which overwhelmed the resonant instability as $\delta \to \max(\delta)$; we also found that $\max(\delta) < \delta_{\max}$, where $\delta_{\max}$ is the highest basic wave amplitude.

With $\Omega_1 \neq 0$, although local K–H instability was still found, $\max(\delta)$ appeared to be determined by two related effects. First, examination of the behaviour of the coefficients $[a_{-M}, \ldots, a_M]$, $M \approx 50$ for $0.05\pi < \delta \leqslant 0.075\pi$, with $\Omega_1 = -10/\pi$ showed some evidence of algebraic-like decay for $1 \ll m < 50$. It is well-known that algebraic decay of the Fourier coefficients of a nearly periodic function defined on a real line (e.g. (4.3)) is characteristic of the near proximity to the real axis of a branch point singularity of the analytically continued function (e.g. see Carrier, Krook & Pearson 1966, p. 256). This can lead at best to very slow convergence of the Fourier expansion of the function, or, at most, to loss of analyticity should the singularity touch the real axis. However, $M = 50$ is far too small for a quantitative test of this possibility by numerical analysis of the moderate- and large-wavenumber Fourier coefficients in (4.3*a–d*). We note that this behaviour is not uncommon in the modelling of surface or interfacial phenomena (Saffman & Yuen 1982).

Secondly, the onset of algebraic-like slow decay of the Fourier coefficients was always accompanied by a rapid decrease in accuracy of the calculated eigenvalues. This can be measured in various ways. For instance, it may be shown from the degeneracy in the choice of P that when P is an odd integer, for an exact calculation all eigenvalues with $\mathrm{Re}\, S \neq 0$ occur as a quartet of independent conjugate pairs, say $(S_k, -S_k^*)$ and $(-S_{-j}, S_{-j}^*)$ for certain indices k and $-j$, where $S_k = S_{-j}$. The difference $|\mathrm{Re}\,(S_k - S_{-j})|$ then gives an estimate of the errors due to round-off and truncation. Indeed, numerical evidence indicated that the error estimate $|\mathrm{Re}\,(S_k - S_{-j})|/\mathrm{Re}\,(S_k)$ calculated with a truncation value of M, was always consistent with the error estimate $|\mathrm{Re}\,(\hat{S}_k - S_k)|/\mathrm{Re}\,(\hat{S}_k)$, where $\hat{S}_k$ is the kth eigenvalue for a truncation value of $\hat{M}(\hat{M} > M)$, and $\hat{M}$ is sufficiently large to ensure convergence with respect to increasing M. For instance, with $D_1 \to \infty$, $\Omega_1 = -10/\pi$, $\delta = 0.07\pi$ and $P = 1$ with $M = 50$ we find that $|\mathrm{Re}\,(S_k - S_{-j})|/\mathrm{Re}\,(S_k) \sim O(10^{-1})$, but for this same case with $\delta = 0.05\pi$, $|\mathrm{Re}\,(S_k - S_{-j})|/\mathrm{Re}\,(S_k) \sim O(10^{-7})$. Thus the possible proximity to the real axis of a branch point singularity leads to a slow convergence of (4.3), giving in turn increased round-off and truncation errors in the eigenvalue solver. Improved accuracy thus requires either a larger value of M, or the use of a higher-precision

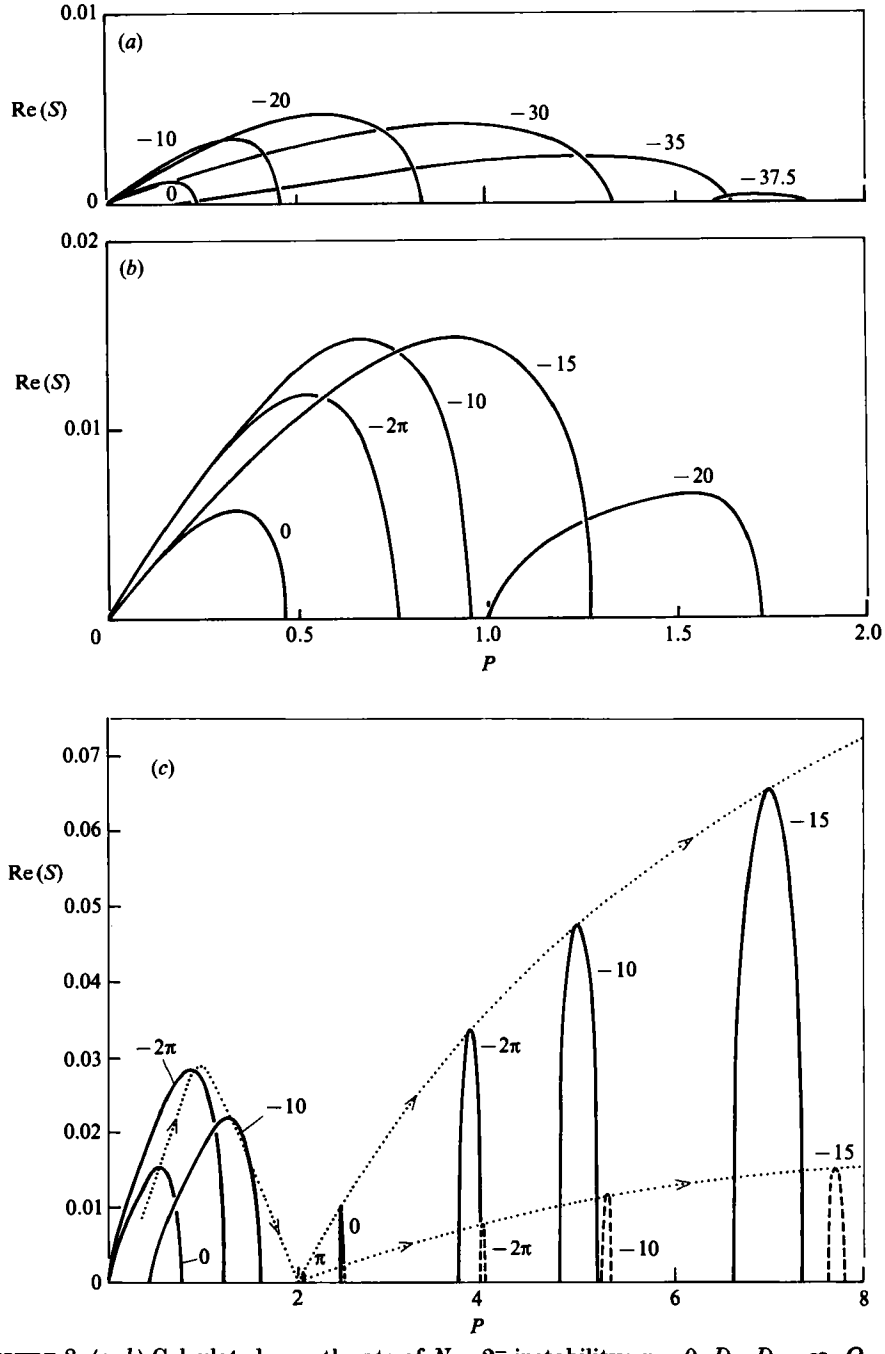

FIGURE 8. (*a*, *b*) Calculated growth rate of $N = 2^-$ instability: $\alpha = 0$, D_1, $D_2 \to \infty$, $\Omega_2 = 0$. Values of $\pi\Omega_1$ shown. (*a*) $\delta/\pi = 0.01$, (*b*) $\delta/\pi = 0.025$. (*c*) Calculated growth rate of $N = 2$ instability: $\alpha = 0$, D_1, $D_2 \to \infty$, $\Omega_2 = 0$. Values of $\pi\Omega_1$ shown. ——, $\delta/\pi = 0.05$; – – – –, $\delta/\pi = 0.025$; ($P = 2^+$); · · · · ·, locus of maximum growth rate; arrows show direction of decreasing Ω_1.

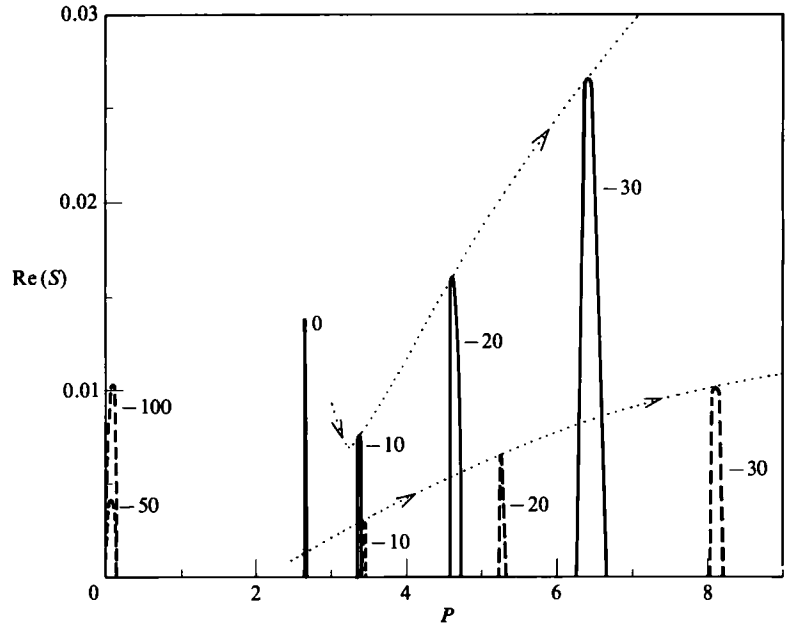

FIGURE 9. Calculated growth rate of $N = 2$ instability: $\alpha = 0$, $D_1 = 0.1\pi$, $D_2 \to \infty$, $\Omega_2 = 0$. Values of $\pi\Omega_1$ shown. For key see figure 8. No $N = 2^-$ instabilities were detected for $\delta/\Omega = 0.05$, $-100/\pi \leqslant \Omega_1 \leqslant 0$.

arithmetic; both these options were impractical with available computing resources. Alternatively, a different representation of η', ϕ_j' and ψ_1', which is more rapidly convergent than (4.3), is needed.

5. Results and discussion

The main results of our numerical calculations are for the $N = 2$ resonant instabilities, and are shown graphically in figures 8–12. We recall that the growth rate of the resonant instability of order N is expected to be $O(\delta^N)$ for small values of the basic wave amplitude δ. A thorough search of the P-axis in the range $0 < P < 2$, for $D_1 \to \infty$, and a range of Ω_1, showed no indication of any instability with $\mathrm{Re}\,(S) \sim O(\delta)$ in the range $0 < \delta \leqslant 0.05\pi$. This is consistent with the result of §2 that there are no one-dimensional $N = 1$ resonances. For the $N = 2$ resonance, some typical resonance curves are shown in figures 2 and 3. From these curves we expect to find two instability bands, one in $0 \leqslant P < 2$ and the other in $P \geqslant 2$. Note that this remains true even when the $N = 2$ resonance curve detaches from the origin of the (P, Q)-plane as $P = Q = 0$ remains an isolated point on the resonance curve (i.e. $P = Q = 0$ is a solution of (2.2)). We shall refer to these two bands as $N = 2^-$ and $N = 2^+$ respectively. The modulational instability theory presented in §3 treated the $N = 2^-$ band for the limit $\delta \to 0$. The present numerical results are a study of $N = 2^-$ and $N = 2^+$ instability bands as functions of D_1, Ω and δ. For $\delta = 0.05\pi$, some $N = 3$ instability bands were detected at values of P near those indicated by the resonance curves in figures 2 and 3. Although these may be more significant at larger values of δ, no systematic study of the $N = 3$ instability bands was attempted here.

In figures 8(a, b) we show the behaviour of the $N = 2^-$ band for the case $D_1 \to \infty$, $\Omega_1 < 0$ (recall that for all the numerical results $D_2 \to \infty$ and $\Omega_2 = 0$). The maximum

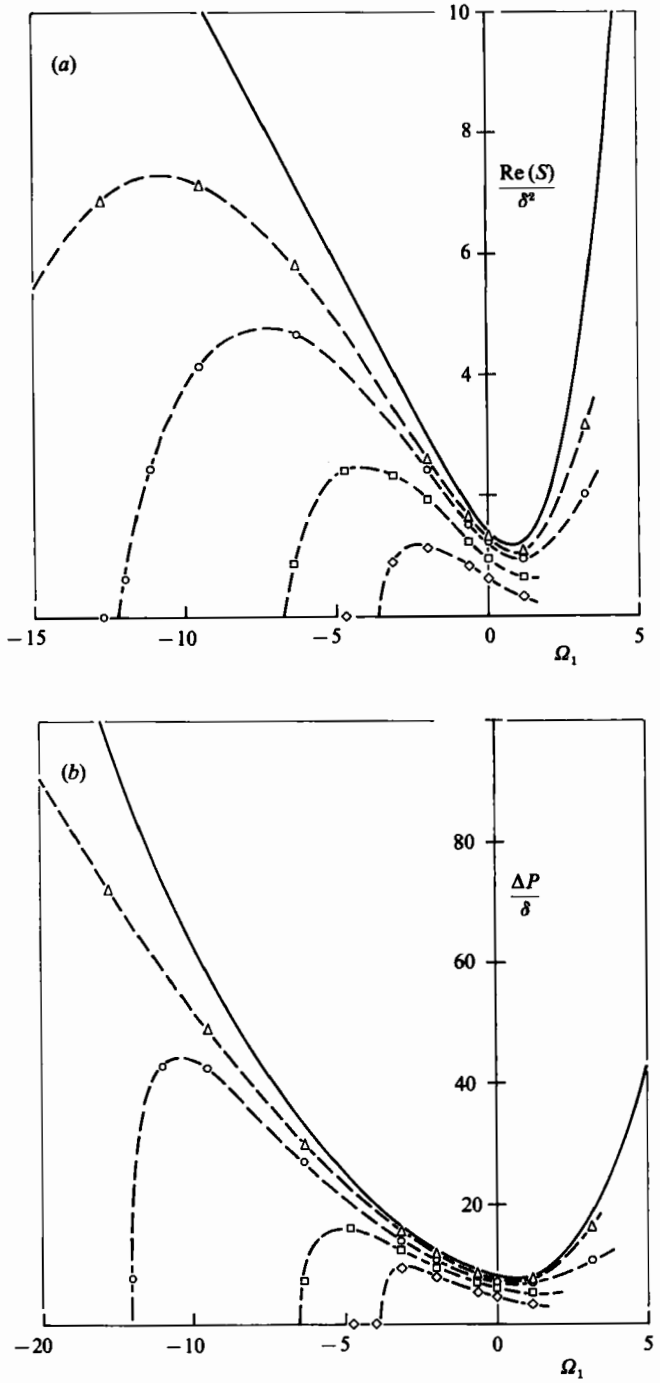

FIGURE 10. (*a*) Maximum growth rate of $N = 2^-$ instability: $\alpha = 0$, D_1, $D_2 \to \infty$, $\Omega_2 = 0$. (*b*) Bandwidth of $N = 2^-$ instability: $\alpha = 0$, D_1, $D_2 \to \infty$, $\Omega_2 = 0$. ——, Modulational instability. Symbols are the numerical results: △, $\delta/\pi = 0.005$; ○, $\delta/\pi = 0.01$; □, $\delta/\pi = 0.025$; ◇, $\delta/\pi = 0.05$.

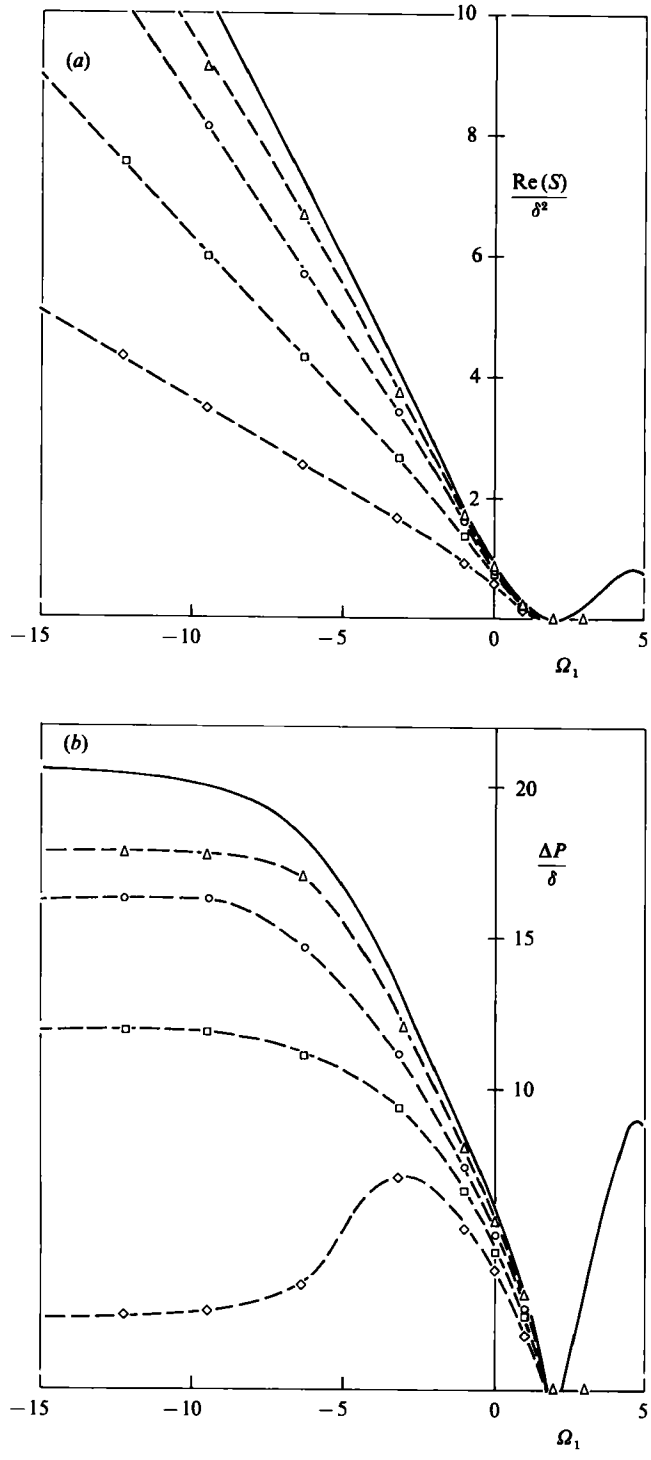

FIGURE 11. (*a*) Maximum growth rate of $N = 2^-$ instability: $\alpha = 0$, $D_1 = 0.5\pi$, $D_1 \to \infty$, $\Omega_2 = 0$. (*b*) Bandwidth of $N = 2^-$ instability: $\alpha = 0$, $D_1 = 0.5\pi$, $D_2 \to \infty$, $\Omega_2 = 0$. For key see figure 10.

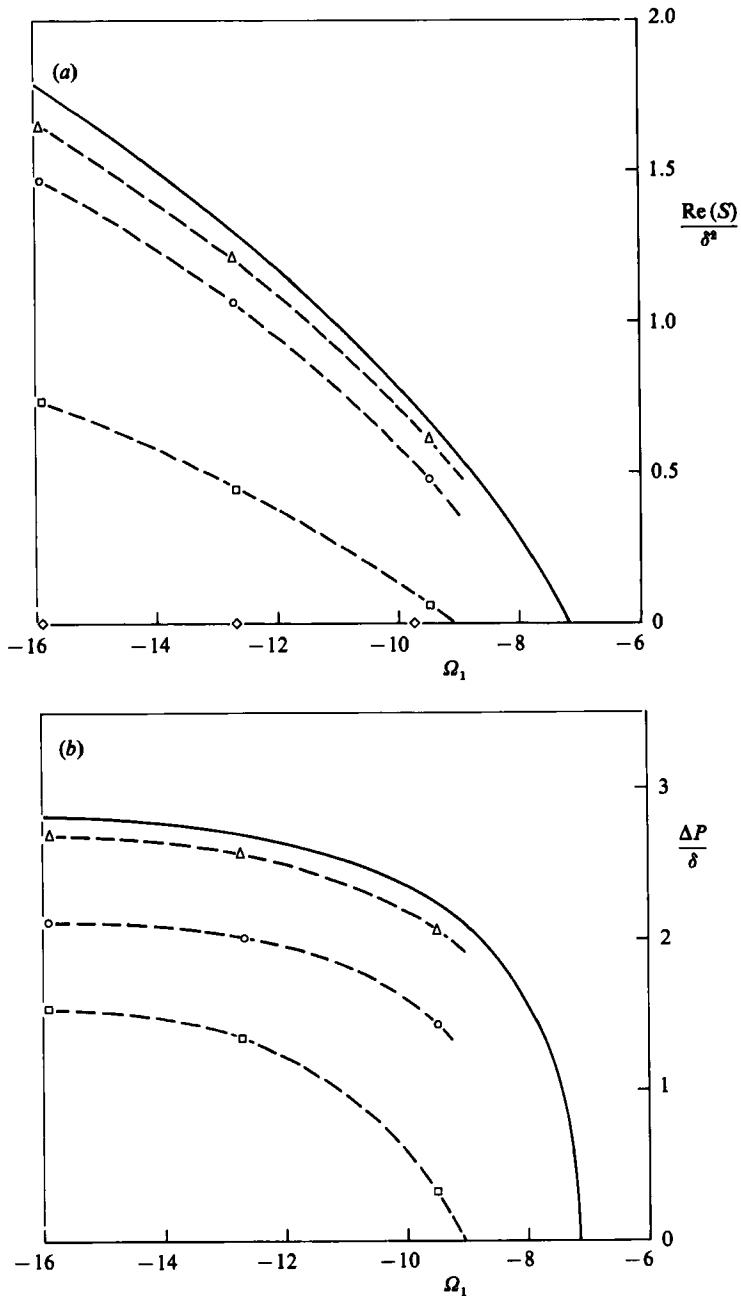

FIGURE 12. (*a*) Maximum growth rate of $N = 2^-$ instability: $\alpha = 0$, $D_1 = 0.1\pi$, $D_2 \to \infty$, $\Omega_2 = 0$. (*b*) Bandwidth of $N = 2^-$ instability: $\alpha = 0$, $D_1 = 0.1\pi$, $D_2 \to \infty$, $\Omega_2 = 0$. For key see figure 10.

growth rate and the bandwidth initially increase with increasing $|\Omega_1|$. For $\Omega_1 \approx -32/\pi$ and $\delta = 0.01\pi$ (figure 8*a*), and for $\Omega_1 \approx -16/\pi$ and $\delta = 0.025\pi$ (figure 8*b*) the $N = 2^-$ band detaches from the origin, and then moves along the positive P-axis, finally contracting and vanishing at $P = 2$. The values of Ω_1 at which the $N = 2^-$ band disappears are indicated in figures 10(*a*, *b*) where we have compared the growth rate, $\mathrm{Re(S)}/\delta^2$, and the bandwidth, $\Delta P/\delta$, with the predictions of the

modulational instability theory of §3. This behaviour is similar to that found for the structure of the $N = 2^-$ band with increasing δ for surface gravity waves on deep water (McLean 1982*a*; Yuen & Lake 1982). However, for this case of surface gravity waves, the whole of the $N = 2$ band contracts into $P = 2$ for sufficiently large δ, and is eventually absorbed by the $N = 3$ band. Here, in contrast, the $N = 2^+$ band increases both in growth rate and in bandwidth while moving to larger values of P in the region $P > 2$ as $|\Omega_1|$ increases; in figure 8(*c*) we give an illustration of this for $\delta = 0.05\pi$. This suggests that, at least for $0 < \delta \leqslant 0.05\pi$, the $N = 2$ band remains of finite extent in the (P, Q)-plane; here, of course, we have only calculated the intersection of the band with the P-axis. It is interesting to note that the value of $\Omega_1 \approx -19$, for which the $N = 2^-$ band disappears at $P = 2$ for $\delta = 0.005\pi$ (the smallest value of δ considered), is similar to the values of Ω_1 for which the $N = 1$ resonance approaches the P-axis at $P = 2$ (see figure 2*a*). We thus speculate that it is the proximity of the $N = 1$ resonance curve to the P-axis that is responsible for the stabilization of the $N = 2^-$ instability band at large values of $-\Omega_1$. In the Appendix we analyse the structure of the quartet equations which describe the $N = 2$ instability for small δ, and show that stabilization is possible as a triad resonance is approached.

In figures 10, 11 and 12 we have compared the numerical predictions of $\max[\mathrm{Re}\,(S)/\delta^2]$ and $\Delta P/\delta^2$ for the $N = 2^-$ instability band with the results from the modulational instability theory of §3 (see figure 4) for the cases $D_1 \to \infty$, 0.5π and 0.1π respectively. The bandwidth is obtained numerically as $\Delta P = P_{\max} - P_{\min}$, where $P_{\max}$, $P_{\min}$ are those points on the P-axis where $\mathrm{Re}\,(S) = 0$ for $N = 2^-$. Generally the trend is for the numerically calculated values of $\mathrm{Re}\,(S)$ and ΔP to grow more slowly than the modulational instability theory would require, viz $O(\delta^2)$ and $O(\delta)$ respectively. However, the validity of the modulational instability theory requires δ small, and $\mathrm{Re}\,(S)/\delta^2$, $\Delta P/\delta$ both $O(1)$, so that the differences for the numerical results will increase for large $|\Omega_1|$, as well as when δ increases.

The detachment of the $N = 2^-$ band from the origin, discussed above for the case $D_1 \to \infty$, also occurs for $D_1 = 0.05\pi$, but at a larger value of $-\Omega_1$ for the same value of δ. However, for this case, the numerical results showed no evidence of contraction of the $N = 2^-$ band towards $P = 2$, at least for $-60/\pi \leqslant \Omega_1 < 0$. With $D_1 = 0.1\pi$, there was again no evidence for detachment of the $N = 2^-$ band from the origin, at least for $-100/\pi \leqslant \Omega_1 < 0$. For this case no $N = 2^-$ instability band was detected for $\delta = 0.05\pi$, although the band exists for $\delta = 0.005\pi$, 0.01π and 0.025π (see figure 9 and figures 12*a*, *b*). However, a vigorous $N = 2^+$ instability band does exist for this amplitude (i.e. $\delta = 0.05\pi$, see figure 9). Referring again to figure 9, we note that the $N = 2^+$ band appears to be approaching $P = 2$ from above as Ω_1 increases, and becomes positive, although this feature is more noticeable for $\delta = 0.025\pi$ than for $\delta = 0.05\pi$. No detailed calculations for $\Omega_1 > 0$ and $D_1 = 0.01\pi$ were attempted. Nevertheless it seems that the general features of the $N = 2$ instability band for $D_1 = 0.01\pi$ are consistent with the resonance curves shown in figures 3(*a*, *b*) and discussed in §2. In particular, the relatively slow approach of the $N = 1$ resonance curve to the P-axis at $P = 2$ compared with the case $D_1 \to \infty$ is consistent with our failure to find detachment of the $N = 2^-$ band from the origin. Also the approach of the $N = 2^+$ resonance curves to $P = 2$ as $\Omega_1 \to \infty$ is consistent with the results of figure 9.

In II (the case $\Omega_1 = 0$) we argued that wave-induced local K–H instability was responsible for the bands of very large unstable eigenvalues that appeared in the spectra for large values of m. Here, with $\Omega_1 \neq 0$, we find qualitatively similar

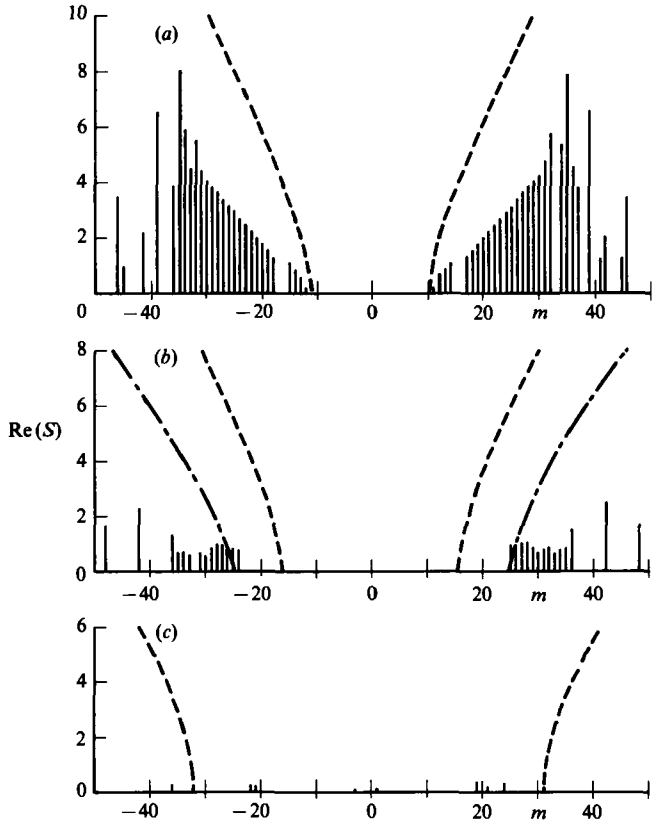

FIGURE 13. Calculated Re(S) spectrum: $\alpha = 0$, D_1, $D_2 \to \infty$, $P = 1.0$, $\delta/\pi = 0.05$, (*a*) $\Omega_1 = 0$, (*b*) $\Omega_1 = -2$, (*c*) $\Omega_1 = -15/\pi$. Only case (*c*) contains a resonant instability at $m = -2, 1$. - - - -, local K–H instability at basic wave crest; – · – · –, local K–H instability at basic wave trough (out of range for (*c*)).

	Basic wave crest		Basic wave trough	
Ω_1	$\bar{U}_1$	$\bar{U}_2$	$\bar{U}_1$	$\bar{U}_2$
0	−0.9408	−0.5067	−0.5067	−0.9408
−2	−1.0348	−0.6518	−1.0284	−1.2882
$-15/\pi$	−1.2447	−0.95031	−1.7921	−1.9548

TABLE 1. Local conditions at the basic wave crest and trough, used in the calculation of the local K–H instability.

behaviour, but interestingly we find that for $\Omega_1 < 0$, as $-\Omega_1$ increases, the growth rate decreases (see figure 13). The mechanism proposed in II may be applied here. Thus, let $\bar{u}_1$, ω_1 and $\bar{u}_2$, ω_2 be the uniform fluid velocity and vorticity respectively above and below an infinite vortex sheet. Then it is readily shown from the appropriate linear dispersion relation (see, for instance, (3.6*c*)), that the complex growth rate $\hat{s}$ of a one-dimensional disturbance of wavelength k is given by (using dimensional coordinates)

$$A\hat{s}^2 + iB\hat{s} + C = 0,$$

where
$$\left.\begin{aligned} A &= \frac{\rho_2 S_2 + \rho_1 S_1}{k}, \\ B &= \frac{\rho_2 \omega_2 - \rho_1 \omega_1}{k} + 2(\rho_2 S_2 \bar{u}_1 + \rho_1 S_1 \bar{u}_2), \\ C &= (\rho_2 - \rho_1) g - (\rho_2 \omega_2 \bar{u}_2 - \rho_1 \omega_1 \bar{u}_1) - k(\rho_2 \bar{u}_2^2 S_2 + \rho_1 \bar{u}_1^2 S_1). \end{aligned}\right\} \tag{5.1}$$

In figure 13 we show the $\mathrm{Re}\,(S)$ spectrum obtained numerically for the case $D_1, D_2 \to \infty$, $\Omega_2 = 0$, $\Omega_1 = 0$, -2 and $-15/\pi$ for $\delta = 0.05\pi$, $P = 1$ and $M = 50$, and compare this with $\mathrm{Re}\,(S)$ calculated from the dimensionless form of (5.1) with $k = 2m + P$, and $\bar{U}_1$, $\bar{U}_2$ obtained from the local values at the basic wave crest and trough. When $\Omega_1 = 0$ local conditions along the upper and lower halves of the basic wave profile are kinematically identical (owing to symmetry) and there is evidently some reinforcement amongst unstable waves generated in each region. However, for $\Omega_1 \neq 0$, conditions at the crest and trough differ. Indeed $|\bar{U}_1 - \bar{U}_2|$ is larger at the crest, leading to the prediction that local K–H instability will occur at lower wavenumbers at the crest, compared with the trough (see figure 13*b*). Figure 13(*b*, *c*) show the attenuation of the strongly unstable eigenvalues at large values of m, as $-\Omega_1$ increases. We have attributed this to the reduction of $|\bar{U}_1 - \bar{U}_2|$ at the wave crest and trough as $-\Omega_1$ increases (see table 1). The poor agreement between the local criterion and the numerically calculated spectra can perhaps be explained by the lack of cooperative reinforcement betwecn local K–H disturbances when crest and trough conditions are different.

6. Conclusions

In this paper we have extended the results of II, for the linearized stability of interfacial waves, to the case when the interfacial waves are propagating on a basic current shear. Although our results are generally restricted to one-dimensional instabilities, it seems clear that for small values of the basic current shear the same interpretation for the instabilities as given in II applies here. Thus, for small or moderate basic wave amplitudes, the instabilities are determined by low-order resonances, with the $N = 2$ resonance being the most dominant. In this respect the results obtained here are similar to the corresponding results obtained for water waves by McLean *et al.* (1981) and McLean (1982*a*, *b*). For larger basic wave amplitudes the dominant instability mechanism is a local wave-induced K–H instability.

However, as the basic current shear is increased some new effects appear. One of the most interesting is discussed in §2 where we show that at sufficiently large negative values of Ω_1 there is transverse $N = 1$ resonance. Although our numerical results are restricted to one-dimensional instabilities, there is good reason to believe that this $N = 1$ resonance will lead to an instability band with growth rates $O(\delta)$ for small values of the basic wave amplitude; if so, this instability would dominate the higher-order resonances. Although our numerical results in this paper are all for interfacial waves in the Boussinesq limit $\alpha \to 0$, the resonance curves calculated in §2 are valid for all values of α, and in particular, are valid as $\alpha \to 1$ which is the limit describing water waves in the presence of basic current shear. Thus our comments made above regarding the $N = 1$ resonance can be applied to this situation also. Our numerical results show that sufficiently large negative values of Ω_1 stabilize one branch of the $N = 2$ instability band. We conjecture that this is caused by the proximity to the P-axis of the $N = 1$ resonance. Although our numerical results are

restricted to one-dimensional instabilities, it seems likely that as the $N = 2$ instability band is stabilized, it is replaced by a stronger, but transverse, $N = 1$ instability band. The effects of very large basic current shear are also apparent in the modulational instability theory of §3, where the stability characteristics showed a strong dependence on Ω_1 and Ω_2. Most notably, the range of validity of the modulational instability theory with respect to the basic wave amplitude is greatly reduced when the basic current shear is large.

The most serious limitation of the present results is the restriction to one-dimensional instabilities (with the exception of the calculation of the resonance curves of §2). Since two-dimensional instabilities are not vorticity-preserving in the presence of basic current shear, it would seem that the formulation used here (and in II) in terms of irrotational flow, cannot be extended to the calculation of two-dimensional instabilities. A new approach is needed, which, at the very least, is likely to be an order-of-magnitude greater in computational complexity. Another limitation of the results obtained here (and in II) is the restriction to interfacial waves as a model of oceanic, or atmospheric, internal waves. We are currently investigating the formulation of a similar problem for waves in continuously stratified fluid.

The contribution of D. I. Pullin to the present work was supported by the Australian Research Grants Scheme under Grant no. F8315031R.

Appendix. Amplitude equations for low-order resonant interactions

Consider a finite set of interacting discrete waves where the nth wave is given, to leading order in ϵ, by

$$\epsilon a_n(t) \exp(\mathrm{i}\boldsymbol{k}_n \cdot \boldsymbol{x} - \mathrm{i}\sigma_n t), \tag{A 1a}$$

where

$$\sigma_n = \sigma(\boldsymbol{k}_n). \tag{A 1b}$$

Here ϵ is a small parameter measuring wave amplitude, $\sigma(\boldsymbol{k})$ is the linear dispersion relation, and we adopt the sign conventions $\sigma(\boldsymbol{k}) = -\sigma(\boldsymbol{k})$, $\boldsymbol{k}_{-n} = -\boldsymbol{k}_n$, and $a_{-n} = a_n^*$. Then for a weakly nonlinear physical system it is well known that the asymptotic differential equations governing the wave amplitudes $a_n(t)$ are (see, for instance, Benney 1962; Benney & Newell 1976; Hasselmann 1966, 1967; Phillips 1960; or Yuen & Lake 1982)

$$\mathrm{i}\frac{\partial a_n}{\partial t} = \epsilon\sigma_n \sum_{l,\,m} f_{lmn}\, a_l^* a_m^* \exp(\mathrm{i}g_n t) + \epsilon^2\sigma_n \sum_{k,\,l,\,m} F_{klmn}\, a_k^* a_l^* a_m^* \exp(\mathrm{i}G_n t) + O(\epsilon^3) \tag{A 2a}$$

where

$$g_n = \sigma_l + \sigma_m + \sigma_n, \tag{A 2b}$$

and

$$G_n = \sigma_k + \sigma_l + \sigma_m + \sigma_n. \tag{A 2c}$$

The coupling coefficients $f_{lmn} = f(\boldsymbol{k}_l, \boldsymbol{k}_m, \boldsymbol{k}_n)$, and $F_{klmn} = F(\boldsymbol{k}_k, \boldsymbol{k}_l, \boldsymbol{k}_m, \boldsymbol{k}_n)$ are non-zero only for those combinations of wavenumbers such that $\boldsymbol{k}_l + \boldsymbol{k}_m + \boldsymbol{k}_n = 0$ or $\boldsymbol{k}_k + \boldsymbol{k}_l + \boldsymbol{k}_m + \boldsymbol{k}_n = 0$ respectively, and satisfy the reality conditions $f_{-l-m-n} = f_{lnm}^*$ and $F_{-k-l-m-n} = F_{klmn}^*$. For a conservative physical system Hasselmann (1966) has shown that they are also symmetric for a suitable choice of amplitudes a_n. The physical system considered in this paper is not necessarily conservative as it is possible for energy to be delivered to the wave field from the basic current shear. Nevertheless, although we have not computed the precise value of the coupling coefficients, some significant conclusions can be drawn from the amplitude equations (A 2a).

First, for a triad resonance g_n is $O(\epsilon)$, and the amplitude equations may be truncated at the ϵ-term (i.e terms of $O(\epsilon^2)$ on the right-hand side can be neglected). The resulting truncated equations can the be used to demonstrate the instability of a basic wave of wavenumber $\boldsymbol{k}_0$ due to resonant interaction with two other waves. In the notation of §2 this is the $N = 1$ resonance, where we identify the triplet $(\boldsymbol{k}_l, \boldsymbol{k}_m, \boldsymbol{k}_n$ with $(\boldsymbol{k}_1, -\boldsymbol{k}_2, \boldsymbol{k}_0)$ (see (2.2)). The basic wave of amplitude a_0 is then perturbed by waves of amplitudes a_1 and a_2. It is then readily shown from the truncated form of (A 2a) that when $|a_1|, |a_2| \ll |a_0|$,

$$\mathrm{i}\frac{\partial a_1}{\partial t} \approx \epsilon 2\sigma_1 f_{-201}\, a_2\, a_0^* \exp(\mathrm{i}gt), \tag{A 3a}$$

$$\mathrm{i}\frac{\partial a_2}{\partial t} \approx \epsilon 2\sigma_2 f_{10-2}^*\, a_1\, a_0 \exp(-\mathrm{i}gt), \tag{A 3b}$$

where

$$g = \sigma_0 + \sigma_1 - \sigma_2. \tag{A 3c}$$

It is readily shown that $a_{1,2}$ are proportional to $\exp(st)$ where the growth rate is given by

$$\{\mathrm{Re}\, s\}^2 = -\tfrac{1}{4}\delta^2 - \epsilon^2 4\sigma_1\sigma_2 f_{-201} f_{10-2}^* |a_0|^2. \tag{A 4}$$

For a conservative system, $f_{-201} = f_{10-2}$ and there is instability whenever $\sigma_1\sigma_2 < 0$ (this argument is due to Hasselmann 1967). In general, whenever (A 4) predicts instability, the instability is centred on the $N = 1$ resonance curve with a bandwidth δ which is $O(\epsilon)$ and a growth rate which is also $O(\epsilon)$.

In the absence of a triad resonance, g_n is bounded away from zero, and to $O(\epsilon)$ the particular solution of (A 2a) for the triad interactions is

$$a_n = -\epsilon\sigma_n \sum_{l,\,m} f_{lmn}\, a_l^*\, a_m^* \frac{\exp(\mathrm{i}g_n t)}{g_n} + O(\epsilon^2). \tag{A 5}$$

When this is substituted into (A 2a) we obtain the following equation for quartet interactions:

$$\mathrm{i}\frac{\partial a_n}{\partial t} = \epsilon^2 \sum_{k,\,l,\,m} \hat{F}_{klmn}\, a_k^*\, a_l^*\, a_m^* \exp(\mathrm{i}G_n t) + O(\epsilon^3), \tag{A 6a}$$

where

$$\hat{F}_{klmn} = \sigma_n F_{klmn} - 2\sum_r \left\{\frac{\sigma_n\sigma_r f_{krn} f_{lm-r}}{\sigma_r - \sigma_l - \sigma_m}\right\}. \tag{A 6b}$$

Here the sum is over all wavenumbers $\boldsymbol{k}_r = \boldsymbol{k}_l - \boldsymbol{k}_m$. We now assume that G_n is $O(\epsilon^2)$, corresponding to a quartet resonance. In the notation of §2 this is the $N = 2$ resonance, and (A 6a) can be used to demonstrate the instability of the basic wave due to a sideband modulation. The argument has been described by Yuen & Lake (1982) and so we give just a brief outline here. The basic wave solution of (A 6a) occurs when the quartet $(\boldsymbol{k}_k, \boldsymbol{k}_l, \boldsymbol{k}_m, \boldsymbol{k}_n)$ is given by $(\boldsymbol{k}_0, -\boldsymbol{k}_0, -\boldsymbol{k}_0, \boldsymbol{k}_0)$ and permutations of the first three wavenumbers. The solution is

$$a_n = \begin{cases} a_0 \exp(\mathrm{i}\nu |a_0|^2 \epsilon^2 t), & \boldsymbol{k}_n = \boldsymbol{k}_0, \\ 0, & \boldsymbol{k}_n \neq \boldsymbol{k}_0, \end{cases} \tag{A 7a}$$

where

$$\nu = -\Sigma\, \hat{F}(\boldsymbol{k}_0, -\boldsymbol{k}_0, -\boldsymbol{k}_0, \boldsymbol{k}_0). \tag{A 7b}$$

Here the sum is over all permutations of the first three arguments, and $\hat{F}(\boldsymbol{k}_k, \boldsymbol{k}_l, \boldsymbol{k}_m, \boldsymbol{k}_n) = \hat{F}_{klmn}$. This is now perturbed by modulations with wavenumbers $\boldsymbol{k}_0 \pm \boldsymbol{p}$ and amplitudes $a_\pm$ corresponding to the quartets $(\boldsymbol{k}_0, -\boldsymbol{k}_0, -\boldsymbol{k}_0 \mp \boldsymbol{p}, \boldsymbol{k}_0 \pm \boldsymbol{p})$ and $(-\boldsymbol{k}_0,$

$-\boldsymbol{k}_0$, $\boldsymbol{k}_0 \mp \boldsymbol{p}$, $\boldsymbol{k}_0 \pm \boldsymbol{p}$) together with permutations of the first three arguments. Here $\boldsymbol{p}$ is the modulation wavenumber defined in §2. The equations governing $a_\pm$ when $|a_\pm| \ll |a_0|$ are

$$\mathrm{i}\frac{\partial a_\pm}{\partial t} = \epsilon^2\beta_\pm |a_0|^2 a_\pm + \epsilon^2\gamma_\pm |a_0|^2 a_\pm^* \exp(2\mathrm{i}Gt + 2\mathrm{i}\nu|a_0|^2\epsilon^2 t), \tag{A 8a}$$

where

$$\beta_\pm = \Sigma\hat{F}(\boldsymbol{k}_0, -\boldsymbol{k}_0, -\boldsymbol{k}_0 \mp \boldsymbol{p}, \boldsymbol{k}_0 \pm \boldsymbol{p}), \tag{A 8b}$$

$$\gamma_\pm = \Sigma\hat{F}(-\boldsymbol{k}_0, -\boldsymbol{k}_0, \boldsymbol{k}_0 \mp \boldsymbol{p}, \boldsymbol{k}_0 \pm \boldsymbol{p}), \tag{A 8c}$$

and

$$2G = \sigma(\boldsymbol{k}_0 + \boldsymbol{p}) + \sigma(\boldsymbol{k}_0 - \boldsymbol{p}) - 2\sigma(\boldsymbol{k}_0). \tag{A 8d}$$

It is now readily shown that $a_\pm$ are proportional to $\exp(st)$ where the growth rate is given by

$$(\mathrm{Re}\, s)^2 = \epsilon^4\gamma_+\gamma_-|a_0|^4 - \tfrac{1}{4}\{2G + \epsilon^2(\beta_+ + \beta_- + 2\nu)|a_0|^2\}^2. \tag{A 9}$$

Here G is an $O(\epsilon^2)$ detuning parameter, and in general (A 9) defines an instability band

$$\epsilon^2 G_-|a_0|^2 < G < \epsilon^2 G_+|a_0|^2, \tag{A 10a}$$

$$G_\pm = \pm(\gamma_+\gamma_-)^{\frac{1}{2}} - \tfrac{1}{2}(\beta_+ + \beta_- + 2\nu). \tag{A 10b}$$

A necessary condition for instability is that $\gamma_+\gamma_- > 0$. In general, whenever (A 9) predicts instability, the instability is centred on the $N = 2$ resonance curve with a bandwidth G that is $O(\epsilon^2)$ (or $O(\epsilon)$ in the modulation wavenumber space, as G is a second-order function of $\boldsymbol{p}$), and a growth rate that is also $O(\epsilon^2)$. Near the origin of the $\boldsymbol{P}$-plane it may be shown from (A 8*b*, *c*) that $\beta_\pm \approx -2\nu$, $\gamma_\pm \approx -\nu$, where ν is given by (A 7*b*), and also

$$G \approx \frac{1}{2}\left\{\frac{\partial^2\sigma}{\partial k^2}(\boldsymbol{k}_0)p^2 + \frac{2\partial^2\sigma}{\partial k\,\partial l}(\boldsymbol{k}_0)pq + \frac{\partial^2\sigma}{\partial l^2}(\boldsymbol{k}_0)q^2\right\}, \tag{A 11}$$

It then follows that (A 9) reduces to

$$(\mathrm{Re}\, s)^2 = G(2\nu\epsilon^2|a_0|^2 - G), \tag{A 12}$$

which is the well-known expression for long-wavelength modulational instability of small-amplitude waves (see, for instance, Davey & Stewartson 1974 or Yuen & Lake 1982). Instability occurs for $G\nu > 0$. In §3 we consider the one-dimensional case ($q = 0$) for the specific physical system of this paper, and calculate the coefficient ν.

We conclude this Appendix by noting the curious fact that if a triad resonance is close in the $\boldsymbol{p}$-plane to a quartet resonance then it may have a stabilizing effect. Indeed, let $g_\pm = \sigma(\boldsymbol{k}_0) \pm \sigma(\boldsymbol{p}) - \sigma(\boldsymbol{k}_0 \pm \boldsymbol{p})$ be the detuning parameters for the triad resonance (see A 3*c*), and let us further suppose that one of $g_\pm$ is small. Then it may be shown from (A 6*b*), where $g_\pm$ occur in the denominator of the second term, that $\beta_\pm$ are proportional to $(g_\pm)^{-1}$ and $\gamma_\pm$ are proportional to $(g_\mp)^{-1}$. It is then apparent from (A 9) that if either of $g_\pm$ is small, there is stability. Some evidence for this behaviour is found in our numerical results of §5. Of course if the triad resonance is approached too closely then it will lead to its own instability given by (A 4).

REFERENCES

Benney, D. J. 1962 Nonlinear gravity wave interactions. *J. Fluid Mech.* **14**, 577–584.

Benney, D. J. & Newell, A. C. 1967 The propagation of nonlinear wave envelopes. *J. Math. Phys.* **46**, 133–139.

Carrier, G. F., Krook, M. & Pearson, G. E. 1966 *Functions of a Complex Variable: Theory and Technique*. McGraw-Hill.

DAVEY, A. & STEWARTSON, D. 1974 On three-dimensional packets of surface waves. *Proc. R. Soc. Lond.* A **338**, 101–110.

GRIMSHAW, R. H. J. & PULLIN, D. I. 1985 Stability of finite-amplitude interfacial waves. Part 1. Modulational instability for small-amplitude waves. *J. Fluid Mech.* **160**, 297–315.

HASSELMANN, K. 1966 Feynman diagrams and interaction rules of wave–wave scattering processes. *Rev. Geophys.* **4**, 1–32.

HASSELMANN, K. 1967 A criterion for nonlinear wave stability. *J. Fluid Mech.* **30**, 737–739.

HOOPER, A. P. & BOYD, W. G. C. 1983 Shear-flow instability at the interface between two viscous fluids. *J. Fluid Mech.* **128**, 507–528.

MCLEAN, J. W. 1982*a* Instabilities of finite-amplitude water waves. *J. Fluid Mech.* **144**, 315–330.

MCLEAN, J. W. 1982*b* Instabilities of finite-amplitude gravity waves on water of finite depth. *J. Fluid Mech.* **114**, 331–341.

MCLEAN, J. W., MA, Y. C., MARTIN, D. U., SAFFMAN, P. G. & YUEN, H. C. 1981 Three-dimensional instability of finite-amplitude water waves. *Phys. Rev. Lett.* **46**, 817–820.

PHILLIPS, O. M. 1960 On the dynamics of unsteady gravity waves of finite amplitude. Part 1. The elementary interactions. *J. Fluid Mech.* **9**, 193–217.

PULLIN, D. I. & GRIMSHAW, R. H. J. 1983*a* Nonlinear interfacial progressive waves near a boundary in a Boussinesq fluid. *Phys. Fluids* **26**, 897–905.

PULLIN, D. I. & GRIMSHAW, R. H. J. 1983*b* Interfacial progressive waves in a two-layer shear flow. *Phys. Fluids* **26**, 1731–1739.

PULLIN, D. I. & GRIMSHAW, R. H. J. 1985 Stability of finite-amplitude interfacial waves. Part 2. Numerical results. *J. Fluid Mech.* **160**, 317–336.

SAFFMAN, P. G. & YUEN, H. C. 1982 Finite-amplitude interfacial waves in the presence of a current. *J. Fluid Mech.* **123**, 459–476.

YUEN, H. C. 1983 Instability of finite-amplitude interfacial waves. In *Waves on Fluid Interfaces* (ed. R. E. Meyer), pp. 17–40. Academic.

YUEN, H. C. & LAKE, B. M. 1982 Nonlinear dynamics of deep-water gravity waves. *Adv. Appl. Mech.* **22**, 67–229.

ZAKHAROV, V. E. 1968 Stability of periodic waves of finite amplitude on the surface of a deep fluid. *J. Appl. Mech. Tech. Phys.* **9**, 190–194.